

Geology of the Northern Norrbotten ore province, northern Sweden

Paper 4 (13)

Editor: Stefan Bergman



SGU

Sveriges geologiska undersökning
Geological Survey of Sweden

Rapporter och meddelanden 141

Geology of the Northern Norrbotten ore province, northern Sweden

Editor: Stefan Bergman

Sveriges geologiska undersökning
2018

ISSN 0349-2176
ISBN 978-91-7403-393-9

Cover photos:

Upper left: View of Torneälven, looking north from Sakkaravaara, northeast of Kiruna. *Photographer:* Stefan Bergman.

Upper right: View (looking north-northwest) of the open pit at the Aitik Cu-Au-Ag mine, close to Gällivare. The Nautanen area is seen in the background. *Photographer:* Edward Lynch.

Lower left: Iron oxide-apatite mineralisation occurring close to the Malmberget Fe-mine. *Photographer:* Edward Lynch.

Lower right: View towards the town of Kiruna and Mt. Luossavaara, standing on the footwall of the Kiruna apatite iron ore on Mt. Kiirunavaara, looking north. *Photographer:* Stefan Bergman.

Head of department, Mineral Resources: Kaj Lax

Editor: Stefan Bergman

Layout: Tone Gellerstedt och Johan Sporrang, SGU

Print: Elanders Sverige AB

Geological Survey of Sweden
Box 670, 751 28 Uppsala
phone: 018-17 90 00
fax: 018-17 92 10
e-mail: sgu@sgu.se
www.sgu.se

Table of Contents

Introduktion (in Swedish)	6
Introduction	7
1.Regional geology of northern Norrbotten County	9
References	14
2. Geology, lithostratigraphy and petrogenesis of c. 2.14 Ga greenstones in the Nunasvaara and Masugnsbyn areas, northernmost Sweden	19
Abstract	19
Introduction	20
Regional setting of Norrbotten greenstone belts	21
Geology of the Nunasvaara and Masugnsbyn greenstone successions	23
Petrogenesis of the greenstones: Preliminary U-Pb geochronology, litho-geochemistry and Sm-Nd isotopic results	52
Summary and conclusions	68
Acknowledgements	69
References	70
3. Stratigraphy and ages of Palaeoproterozoic metavolcanic and metasedimentary rocks at Käymäjärvi, northern Sweden	79
Abstract	79
Introduction	80
General geology	80
Structure and stratigraphy of the Käymäjärvi area	81
Sample description	89
Analytical methods	90
Analytical results	91
Discussion	96
Conclusions	100
Acknowledgements	101
References	101
4. Petrological and structural character of c. 1.88 Ga meta-volcanosedimentary rocks hosting iron oxide-copper-gold and related mineralisation in the Nautanen–Aitik area, northern Sweden	107
Abstract	107
Introduction	108
Regional setting	108
Geology of the Nautanen–Aitik area	110
Structural geology and deformation	132
Summary and Conclusions	144
Acknowledgements	144
References	145
5. Age and lithostratigraphy of Svecofennian volcanosedimentary rocks at Masugnsbyn, northernmost Sweden – host rocks to Zn-Pb-Cu- and Cu ±Au sulphide mineralisations	151
Abstract	151
Introduction	152
Geological overview	153
Discussion and preliminary conclusions	194
Acknowledgements	197
References	198

6. Folding observed in Palaeoproterozoic supracrustal rocks in northern Sweden	205
Abstract	205
Introduction	205
Geological setting	207
Structural geological models	209
Geophysical data	212
Discussion and Conclusions	251
References	255
7. The Pajala deformation belt in northeast Sweden:	
Structural geological mapping and 3D modelling around Pajala	259
Abstract	259
Geological setting	259
Structural analysis	263
2D regional geophysical modelling and geological interpretation	272
Local and semi-regional 3D models	274
Discussion	280
Conclusions	283
References	284
8. The Vakko and Kovo greenstone belts north of Kiruna:	
Integrating structural geological mapping and geophysical modelling	287
Abstract	287
Introduction	287
Geological setting	289
Geophysical surveys	291
Results	296
Discussion	306
Conclusions	308
References	309
9. Geophysical 2D and 3D modelling in the areas around	
Nunasvaara and Masugnsbyn, northern Sweden	311
Abstract	311
Nunasvaara	312
2D modelling of profile 1 and 2	316
Masugnsbyn	321
Regional modelling	329
Conclusion	338
References	339
10. Imaging deeper crustal structures by 2D and 3D modelling of geophysical data.	
Examples from northern Norrbotten	341
Abstract	341
Introduction	341
Methodology	342
Geological setting	342
Results	345
Conclusion	358
Outlook	358
Acknowledgements	358
References	359

11. Early Svecokarelian migmatisation west of the Pajala deformation belt, northeastern Norrbotten province, northern Sweden	361
Abstract	361
Introduction	362
Geology of the Masugnsbyn area	362
Discussion	372
Conclusions	374
Acknowledgements	375
References	376
12. Age and character of late-Svecokarelian monzonitic intrusions in northeastern Norrbotten, northern Sweden	381
Abstract	381
Introduction	381
Geological setting	382
Analytical methods	387
Analytical results	388
Discussion	393
Conclusions	396
Acknowledgements	396
References	397
13. Till geochemistry in northern Norrbotten –regional trends and local signature in the key areas	401
Abstract	401
Introduction	401
Glacial geomorphology and quaternary stratigraphy of Norrbotten	403
Samples and methods	406
Results and discussion	407
Conclusions	426
Acknowledgements	427
References	427

Introduktion

Stefan Bergman & Ildikó Antal Lundin

Den här rapporten presenterar de samlade resultaten från ett delprojekt inom det omfattande tvärvetenskapliga Barentsprojektet i norra Sverige. Projektet initierades av Sveriges geologiska undersökning (SGU) som ett första led i den svenska mineralstrategin. SGU fick ytterligare medel av Näringsdepartementet för att under en fyraårsperiod (2012–2015) samla in nya geologiska, geofysiska och geokemiska data samt för att förbättra de geologiska kunskaperna om Sveriges nordligaste län. Det statligt ägda gruvbolaget LKAB bidrog också till finansieringen. Projektets strategiska mål var att, genom att tillhandahålla uppdaterad och utförlig geovetenskaplig information, stödja prospekterings- och gruvindustrin för att förbättra Sveriges konkurrenskraft inom mineralnäringen. Ny och allmänt tillgänglig geovetenskaplig information från den aktuella regionen kan hjälpa prospekterings- och gruvföretag att minska sina risker och prospekteringskostnader och främjar därigenom ekonomisk utveckling. Dessutom bidrar utökad geologisk kunskap till en effektiv, miljövänlig och långsiktigt hållbar resursanvändning. All data som har samlats in i projektet lagras i SGUs databaser och är tillgängliga via SGU.

Syftet med det här delprojektet var att få en djupare förståelse för den stratigrafiska uppbyggnaden och utvecklingen av de mineraliserade ytbergarterna i nordligaste Sverige. Resultaten, som är en kombination av ny geologisk kunskap och stora mängder nya data, kommer att gynna prospekterings- och gruvindustrin i regionen i många år framöver.

Norra Norrbottens malmprovins står för en stor del av Sveriges järn- och kopparmalmsproduktion. Här finns fyra aktiva metallgruvor (mars 2018) och mer än 500 dokumenterade mineraliseringar. Fyndigheterna är av många olika slag, där de viktigaste typerna är stratiforma kopparmineraliseringar, järnformationer, apatitjärnmalm av Kirunatyp och epigenetiska koppar-guldmineraliseringar. En vanlig egenskap hos de flesta malmer och mineraliseringar i Norr- och Västerbotten är att de har paleoproterozoiska vulkaniska och sedimentära bergarter som värdbergart. För undersökningarna valdes ett antal nyckelområden med bästa tillgängliga blottningsgrad. De utvalda områdena representerar tillsammans en nästan komplett stratigrafi i ytbergarter inom åldersintervallet 2,5–1,8 miljarder år.

Rapporten består av tretton kapitel och inleds med en översikt över de geologiska förhållandena, som beskriver huvuddragen i de senaste resultaten. Översikten följs av fyra kapitel (2–5) som huvudsakligen handlar om litostratigrafi och åldersbestämningar av ytbergarterna. Huvudämnet för de därpå följande fem kapitlen (6–10) är 3D-geometri och strukturell utveckling. Därefter kommer två kapitel (11–12) som fokuserar på U-Pb-datering av en metamorf respektive intrusiv händelse. Rapporten avslutas med en studie av geokemin hos morän i Norra Norrbottens malmprovins (kapitel 13).

Introduction

Stefan Bergman & Ildikó Antal Lundin

This volume reports the results from a subproject within the Barents Project, a major programme in northern Sweden. The multidisciplinary Barents Project was initiated by SGU as the first step in implementing the Swedish National Mineral Strategy. SGU obtained additional funding from the Ministry of Enterprise and Innovation to gather new geological, geophysical and till geochemistry data, and generally enhance geological knowledge of northern Sweden over a four-year period (2012–2015). The state-owned iron mining company LKAB also helped to fund the project. The strategic goal of the project was to support the exploration and mining industry, so as to improve Sweden's competitiveness in the mineral industry by providing modern geoscientific information. Geological knowledge facilitates sustainable, efficient and environmentally friendly use of resources. New publicly available geoscientific information from this region will help exploration and mining companies to reduce their risks and exploration costs, thus promoting economic development. All data collected within the project are stored in databases and are available at SGU.

This subproject within the Barents Project aims to provide a deeper understanding of the stratigraphy and depositional evolution of mineralised supracrustal sequences in northernmost Sweden. The combined results in the form of new geological knowledge and plentiful new data will benefit the exploration and mining industry in the region for many years to come.

The Northern Norrbotten ore province is a major supplier of iron and copper ore in Sweden. There are four active metal mines (March 2018) and more than 500 documented mineralisations. A wide range of deposits occur, the most important types being stratiform copper deposits, iron formations, Kiruna-type apatite iron ores and epigenetic copper-gold deposits. A common feature of most deposits is that they are hosted by Palaeoproterozoic metavolcanic or metasedimentary rocks. A number of key areas were selected across parts of the supracrustal sequences with the best available exposure. The areas selected combine to represent an almost complete stratigraphic sequence.

This volume starts with a brief overview of the geological setting, outlining some of the main recent achievements. This is followed by four papers (2–5) dealing mainly with lithostratigraphy and age constraints on the supracrustal sequences. 3D geometry and structural evolution are the main topics of the next set of five papers (6–10). The following two contributions (11–12) focus on U-Pb dating of a metamorphic event and an intrusive event, respectively. The volume concludes with a study of the geochemical signature of till in the Northern Norrbotten ore province (13).

Authors, paper 4:

Edward P. Lynch

Geological Survey of Sweden
Department of Mineral Resources
Uppsala, Sweden

Tobias E. Bauer

Luleå University of Technology,
Division of Geosciences and Environmental Engineering,
Luleå, Sweden

Johan Jönberger

Geological Survey of Sweden
Department of Mineral Resources
Uppsala, Sweden

Zmar Sarlus

Luleå University of Technology,
Division of Geosciences and Environmental Engineering,
Luleå, Sweden

George A. Morris

Geological Survey of Sweden
Department of Mineral Resources
Uppsala, Sweden

Per-Olof Persson

Swedish Museum of Natural History,
Department of Geosciences,
Stockholm, Sweden

4. Petrological and structural character of c. 1.88 Ga meta-volcanosedimentary rocks hosting iron oxide-copper-gold and related mineralisation in the Nautanen–Aitik area, northern Sweden

Edward P. Lynch, Tobias E. Bauer, Johan Jönberger, Zmar Sarlus, George A. Morris & Per-Olof Persson

ABSTRACT

The petrological and deformation characteristics of a Palaeoproterozoic meta-volcanosedimentary sequence in the Nautanen–Aitik area (near Gällivare, northern Sweden) are presented. The investigated sequence (part of the *Muorjevaara group*) predominantly comprises metavolcaniclastic rocks displaying variable grain size, textural and syn-depositional features (e.g. grading, cross-laminae, compositional banding). Locally, poorly sorted agglomerate-like horizons with coarser clasts (lapilli- to block-size) occur. Interbedded sections of mainly fine-grained, volcanogenic (epiclastic) metasedimentary rocks contain syn-depositional features that suggest a sub-aqueous, relatively shallow depositional environment. Locally preserved cross-laminae in this unit provide evidence of way-up and paleocurrent directions. Intercalations of pelite, mica schist and amphibolitic schist also occur throughout the sequence. In general, least altered samples indicate a predominantly intermediate (basaltic andesitic to andesitic), calc-alkaline composition for the sequence.

U-Pb SIMS zircon dating of a meta-andesite horizon, intercalated within the sequence, has yielded a precise U-Pb concordia age of 1878 ± 7 Ma (2σ , $n=12$). This date constrains the timing of intermediate volcanism and the deposition of syn-volcanic epiclastic material. By inference, it also provides an estimate for the age of *Muorjevaara group* rocks hosting the Nautanen Cu-Au and Aitik Cu-Au-Ag deposits. When combined with lithogeochemical signatures, the new age also confirms a genetic link between the metavolcaniclastic package and gabbroic to dioritic intrusions in the area (e.g. the c. 1.88 Ga Aitik stock). Additionally, several zircon cores record $^{207}\text{Pb}/^{206}\text{Pb}$ apparent ages between c. 1.90 and 1.89 Ga, suggesting inheritance of marginally older volcanic \pm plutonic material not exposed at the present erosion level.

The Nautanen–Aitik area contains the roughly north-northwest-trending *Nautanen deformation zone* (NDZ), a major composite brittle-ductile structure hosting hydrothermal iron oxide-Cu-Au (IOCG)-style mineralisation (e.g. the Nautanen deposit). Here, the bedrock is relatively intensely altered and sheared, and has been transposed into a sub-parallel high-strain zone predominantly consisting of a composite planar penetrative fabric. Outside the high-strain zone, relatively large-scale approximately North-northwest-aligned folds and discordant brittle structures occur. Magnetic susceptibility and VLF-resistivity modelling of the NDZ confirm that composite planar structures mainly dip steeply to the west-southwest and continue at depth.

INTRODUCTION

The composite Sveco Karelian orogeny (the name Svecofennian is also used) is recognised as a major period of crustal reworking and growth on the margins of the Fennoscandian Shield during the Palaeoproterozoic (e.g. Nironen 1997, Korja et al. 2006, Lahtinen et al. 2009). In northernmost Sweden (Norrbotten), c. 1.95–1.78 Ga volcanic, sedimentary and intrusive rocks (and their related structures) record a protracted and episodic phase of accretionary orogenesis and crustal amalgamation during a major phase of tectonic convergence, metamorphism and magmatism (e.g. Bergman et al. 2001, Weihed et al. 2005, Bergman et al. 2006).

Regional assessments of Paleoproterozoic metasedimentary rocks across Norrbotten (i.e. metamorphosed volcanosedimentary cover sequences) have helped establish a lithostratigraphic framework for the area and provide a lithotectonic context for its metallogenic evolution (e.g. Bergman et al. 2001, Martinsson 2004, Martinsson et al. 2016). However, detailed, local-scale investigations of specific sequences and associated structures at key stratigraphic intervals are generally lacking (cf. Monro 1988, Edfelt et al. 2006, Wanhainen et al. 2006). Such investigations are warranted in Norrbotten, given the association of volcanosedimentary basins and transecting ductile-brittle deformation zones with hydrothermal base and precious metal mineralisation (e.g. Smith et al. 2007, Smith et al. 2009, Wanhainen et al. 2012, Smith et al. 2013).

In this study, we present the results of a targeted investigation of Paleoproterozoic (Orosirian) meta-supracrustal rocks occurring in the Nautanen–Aitik area near Gällivare in northern Norrbotten (Fig. 1). The study area contains a partly conformable and polydeformed meta-volcanosedimentary succession (part of the *Muorjevaara group*), transected by a major deformation zone hosting iron oxide-copper-gold (IOCG)-style mineralisation. Bedrock and structural mapping, ground geophysical data, lithogeochemistry and U-Pb SIMS zircon geochronology are integrated to provide an assessment of the petrological, deformation and mineralisation characteristics of the area. The results presented here complement an earlier account of the geology of the study area reported by Lynch et al. (2015).

In this account, the “Nautanen area” corresponds to the study area outlined in Figure 2 and extends beyond the historical Nautanen Cu-Au mine and the Nautanen deformation zone. For practical, descriptive and geological reasons, we have subdivided the main study area into three lithological-structural domains (Fig. 2). From east to west they are (1) the eastern volcanosedimentary domain (EVD, Muorjevaara to Linaälven area); (2) the central Nautanen deformation zone domain (NDZ domain); and (3), the western volcanosedimentary domain (WVD, Pahtavaara-Huivijokki area).

REGIONAL SETTING

The oldest rocks in northern Norrbotten are Meso- to Neoarchaeal gneisses and metagranitoids, which constitute a partially hidden basement complex extending roughly from Luleå in the south to Sweden’s northern border (Fig. 1, Öhlander et al. 1987, Martinsson et al. 1999, Mellqvist et al. 1999). The Archaean basement forms part of the larger *Norrbotten craton* (Lahtinen et al. 2005, Lauri et al. 2016), a continental terrane, which at c. 2.5 Ga formed part of a composite supercontinent called *Kenorland* (e.g. Reddy & Evans 2009, Melezhik et al. 2012). The Norrbotten craton subsequently broke away from Kenorland during lithospheric-scale rifting and continental dispersal commencing at c. 2.45 Ga (e.g. Hanski & Huhma 2005, Lahtinen et al. 2008, Melezhik & Hanski 2012).

Intracontinental rifting and extension of the Norrbotten craton between c. 2.4 and 2.1 Ga resulted in the deposition of Karelian supracrustal rocks onto the Archaean basement (e.g. Bergman et al. 2001). Early rift-related Karelian successions mainly consist of clastic metasedimentary rocks (meta-conglomerate, quartzite) and subordinate mafic to intermediate metavolcanic rocks. Later-stage Karelian successions consist of abundant mafic metavolcanic and intrusive rocks (tholeiitic to minor komatiitic varieties), and intercalated metasedimentary rocks (black schist, marble, meta-ironstone, pelite,

metachert). These later successions combine to form the northern Norrbotten greenstone belts, part of a Palaeoproterozoic large igneous province occurring across Fennoscandia (Fig. 1, Martinsson 1997, Melezhik & Fallick 2010, Lynch et al., 2018b; cf. Hanski 2012).

Metavolcanic and metasedimentary successions formed between c. 1.9 and 1.8 Ga during the composite Svecokarelian orogeny are the most abundant Palaeoproterozoic metasupracrustal rocks in northern Norrbotten (Fig. 1). Svecofennian successions mainly consist of calc-alkaline to alkaline, intermediate to felsic metavolcanic rocks and associated epiclastic and metasedimentary sequences (Martinsson 2004). In general, these syn-orogenic rocks are considered to have been deposited, deformed and metamorphosed (up to middle amphibolite facies) within an evolving continental arc-type setting during northward-directed subduction, arc-continent accretion and continent-continent collision (e.g. Lahtinen et al. 2005, Lahtinen et al. 2009, Melezhik et al. 2012).

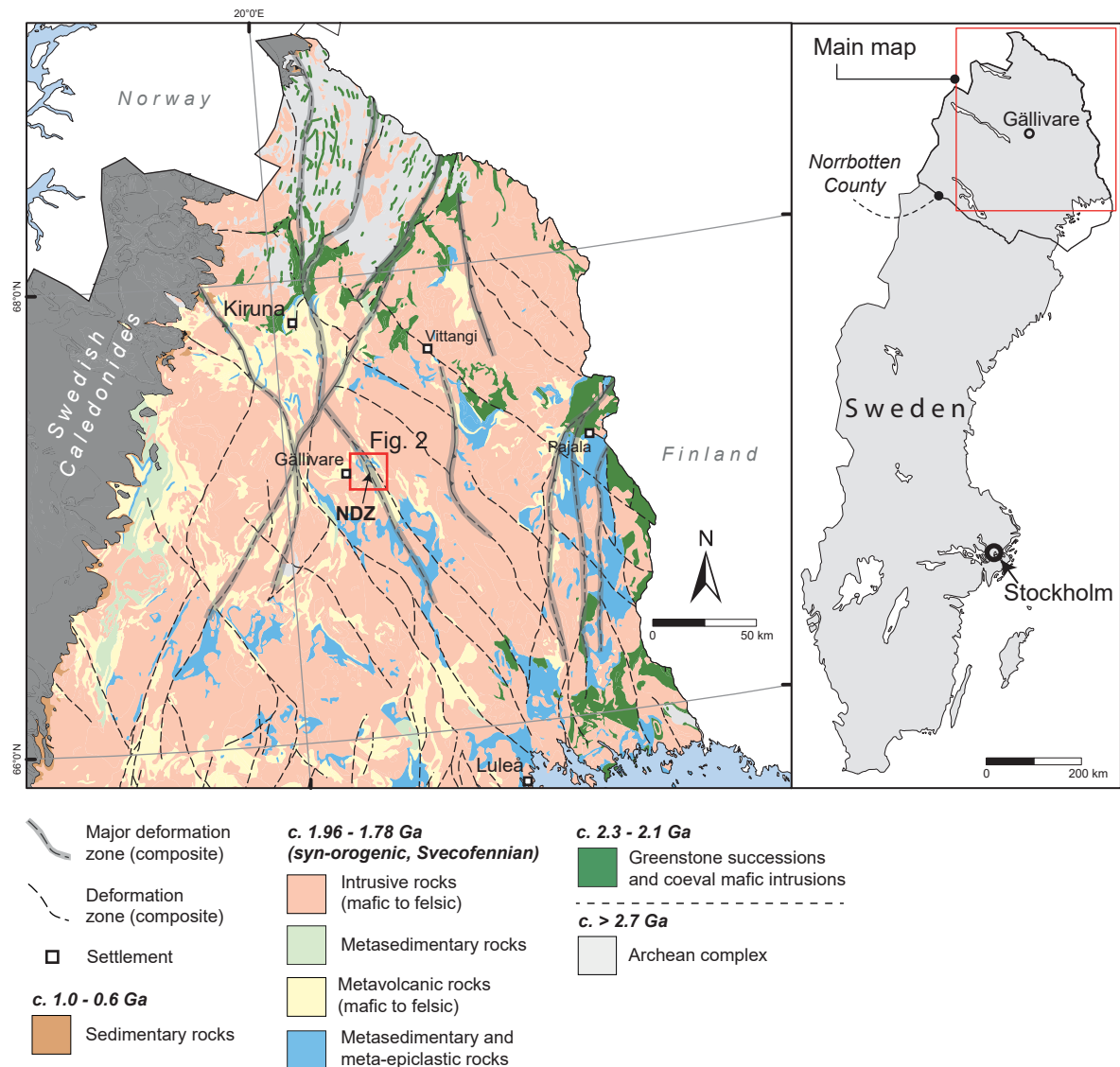


Figure 1. Regional geology of northernmost Sweden (Norrbotten). The red rectangle in the main map represents the Nautanen–Aitik area, corresponding to Figure 2. NDZ = Nautanen deformation zone. Base geology is from Bergman et al. (2012). Major deformation zones are from Bergman et al. (2001).

Across northern Norrbotten, Palaeoproterozoic metasupracrustal successions are surrounded and enclosed by voluminous, syn- to late-orogenic intrusive rocks (Fig. 1). In general, five main intrusive suites or associations are recognised (cf. Ahl et al. 2001, Bergman et al. 2001). These are (1) c. 1.89–1.86 Ga gabbros and dioritoids assigned to the *Haparanda* suite; (2) c. 1.88–1.86 Ga gabbros, syenitoids and granitoids assigned to the *Perthite monzonite* suite; (3) c. 1.86–1.84 Ga granitoids; (4) c. 1.81–1.78 Ga granitic rocks of the *Lina* suite; and (5) c. 1.80 Ga and possibly younger gabbro-dolerite intrusions (cf. Sarlus 2016).

The westernmost margin of northern Norrbotten is marked by Neoproterozoic sedimentary cover rocks and the approximately northeast-trending, low-angle nappe stacks of the Swedish Caledonides, which rest unconformably on the Archaean to Palaeoproterozoic shield area (e.g. Corfu et al. 2014).

GEOLOGY OF THE NAUTANEN–AITIK AREA

The Nautanen–Aitik area is centred on a partly conformable succession of syn-orogenic, Palaeoproterozoic meta-volcanosedimentary rocks (Fig. 2; Witschard 1996). The metasupracrustal sequence is generally of calc-alkaline, basaltic andesite to andesite composition and has undergone extensive deformation, metamorphism, recrystallisation and hydrothermal alteration (McGimpsey 2010, Waara 2015, Lynch et al. 2015).

A variety of intrusive rocks occur across the area, including deformed gabbroic, syenitic and dioritic bodies and younger, deformed to massive granitic and gabbroic-doleritic plutons and dykes (e.g. Wanhainen et al. 2006, Sarlus 2016). Two fairly large, sub-rounded, mafic-ultramafic intrusions named the Dundret and Vasaravaara complexes occur further east near Gällivare. These rocks exhibit distinct cumulate zones defining a primary magmatic layering consisting of olivine, pyroxene and plagioclase in varying proportions (Sarlus 2016).

Metasupracrustal rocks in the general Gällivare area host the Malmberget iron mine, Sweden's second largest iron resource after the Kiirunavaara deposit in Kiruna, and the Aitik Cu-Au-Ag deposit, one of Europe's largest copper mines (Fig. 2, e.g. Lund 2009, Wanhainen et al. 2012). Additionally, several hydrothermal Cu-Au occurrences assigned to the “iron oxide-copper-gold (IOCG)” mineral deposit class occur within a major approximately north-northwest-trending composite shear zone termed the Nautanen deformation zone (cf. Smith et al. 2013, Drejing-Carroll et al. 2015). Episodic deformation along this zone probably enhanced permeability and hydrothermal fluid flow, resulting in a relatively focused, linear zone of alteration and mineralisation (cf. Witschard 1996).

Metamorphic mineral assemblages and pressure-temperature (PT) estimates suggest the area reached middle amphibolite facies conditions during peak regional metamorphism. Bergman et al. (2001) noted a major metamorphic grade boundary in the area, with rocks east of the Nautanen deformation zone having a lower grade than those within the zone and to the west. Tollefsen (2014) reported PT estimates for regional metamorphism from approximately 550 to 660°C and 2 to 5 kbar (i.e. lower to middle amphibolite facies), contact metamorphism adjacent to Lina-type granite (forming a sillimanite-biotite-muscovite assemblage) between approximately 630 and 710°C and 2.0 to 4.4 kbar, and retrograde conditions between approximately 430 and 570°C, and 3.0 to 3.5 kbar. Additionally, Waara (2015) obtained PT estimates of approximately 630–680°C and 6.5 kbars for metasomatic garnet growth associated with potassic-ferroan alteration and Cu-Au mineralisation at the Nautanen deposit (equivalent to middle amphibolite facies conditions).

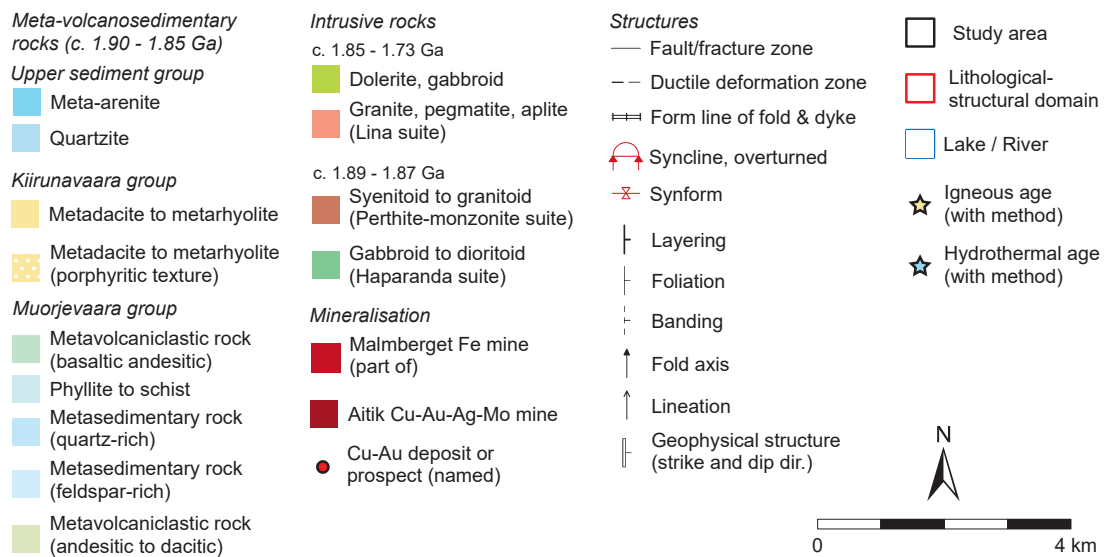
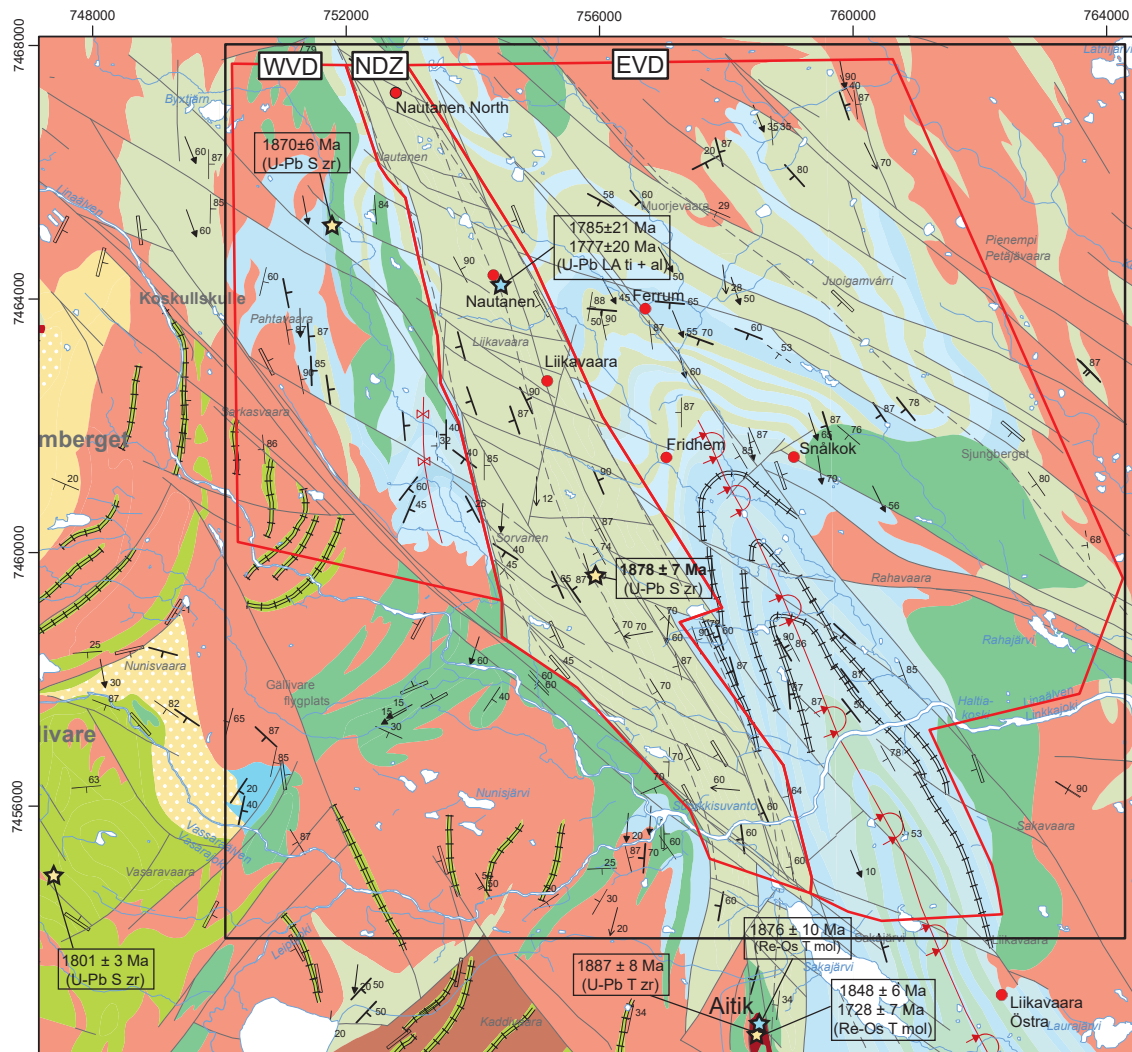


Figure 2. Geology of the Aitik–Gällivare area (modified after Witschard 1996). Abbreviations: EVD = eastern volcanosedimentary domain; NDZ = Nautanen deformation zone (domain); WVD = western volcanosedimentary domain. Geochronology abbreviations and sources: U-Pb S zr = U-Pb SIMS zircon dating (Sarlus 2016, and this study = highlighted bold text in NDZ), U-Pb T zr = U-Pb TIMS zircon dating (Wanhainen et al. 2006), Re-Os T mol = Re-Os TIMS molybdenite dating (Wanhainen et al. 2005), U-Pb T ti = U-Pb TIMS titanite dating (Wanhainen et al. 2009), U-Pb LA ti + al = U-Pb laser ablation-inductively coupled-mass spectrometry titanite and allanite dating (Smith et al. 2009).

Stratigraphy and correlations with other Svecofennian successions

A schematic stratigraphy of the Gällivare area is presented in Figure 3 and follows the system outlined in Lynch et al. (2015) and references therein. The informal stratigraphic units *Muorjevaara group*, *Kiirunavaara group* and *Upper sediment group* are retained here.

Stratigraphically, the *Muorjevaara group* represents a basal, mainly calc-alkaline volcanosedimentary sequence. This is overlain by the *Kiirunavaara group*, comprising alkalic (trachytic) intermediate to acidic metavolcanic rocks (Martinsson & Wanhainen 2004). This unit hosts the iron oxide-apatite deposit at Malmberget (e.g. Lund 2009). Finally, local quartzite outliers of the *Upper sediment group* represent the uppermost stratigraphic unit. In the absence of outcropping transitional contacts, the major stratigraphic units are inferred to be separated by unconformities. The *Muorjevaara* and *Kiirunavaara* groups partly correspond to the regional *Porphyrite* and *Porphyry groups* of Bergman et al. (2001), respectively (Fig. 3). Traditionally, these regional stratigraphic units have been considered broadly coeval and have mainly been divided on the basis of petrographic and geochemical considerations (cf. Perdahl 1995).

Regional correlations between Muorjevaara group rocks and equivalent meta-volcanosedimentary successions elsewhere in northern Norrbotten are permissible based on broad lithological criteria (e.g. Ros 1980, Martinsson 1995). Inferred correlative successions include (roughly from west to east, Fig. 3) (1) Kilavaara Group schist, amphibolite and quartzite in the Svapavaara-Vittangi area (Eriksson & Hallgren 1975); (2) Ruutivaara and Haaravaara Group paragneiss and amphibolite in the Lainio area (Witschard 1970); (3) Pahakurkio Group schist, amphibolite and quartzite in the Tärendö area (Padget 1970); and (4) Sammakkovaara Group schist and metavolcaniclastic rocks in the Pajala area (Padget 1977, Martinsson 2004). In the last-mentioned case, correlation with the Sammakkovaara Group and related metavolcaniclastic rocks is supported by similar litho-geochemical signatures (cf. Luth et al. 2015). A correlation between the Muorjevaara group and rocks of the Kurravaara conglomerate unit in the Kiruna area has also been proposed (Ros 1980; cf. Offerberg 1967).

The Nautanen Deformation Zone and related iron oxide-copper-gold mineralisation

The Nautanen–Aitik area contains a regionally significant, roughly north-northwest-trending ductile-brittle shear zone named the Nautanen deformation zone (NDZ; Witschard 1996). It represents the most conspicuous structural feature in the area and is clearly delineated on magnetic anomaly maps as a somewhat dilational, linear zone of sub-parallel and tightly banded magnetic susceptibility anomalies (see *Geophysical modelling* section). The coupling of high-strain deformation and magnetic banding reflects episodic metasomatic-hydrothermal fluid flow, probably enhanced by increased permeability associated with protracted and focused deformation (e.g. Pitkänen 1997, Smith et al. 2013).

Based on regional structural and magnetic lineament geometries, Bergman et al. (2001) assigned a dextral-oblique shear sense to the NDZ, with a southwest-side up reverse component. Earlier geological mapping and geophysical measurements within the shear zone also identified several sub-parallel, north-northwest-orientated, moderately plunging folds (e.g. Gustafsson 1986, Pitkänen 1997). Internally, the deformation zone is characterised by moderate to intense shearing, mylonitisation, structural transposition and pervasive metasomatic-hydrothermal alteration (see further discussion in the *Structural geology and deformation* section).

Meta-volcanosedimentary rocks within and adjacent to the NDZ host several replacement and vein-related (epigenetic-style) Cu ± Au deposits and prospects (see reviews by Martinsson & Wanhainen 2004, Martinsson & Wanhainen 2013). Important examples include the Nautanen, Liikavaara and Ferrum prospects (Fig. 2). Two general styles of mineralisation are recognised (e.g. Gustafsson 1985, Martinsson & Wanhainen 2004): (1) an inferred older phase of disseminated to semi-massive (replacement-style) sulphide mineralisation forming sub-vertical, lenses and linear zones mainly within the

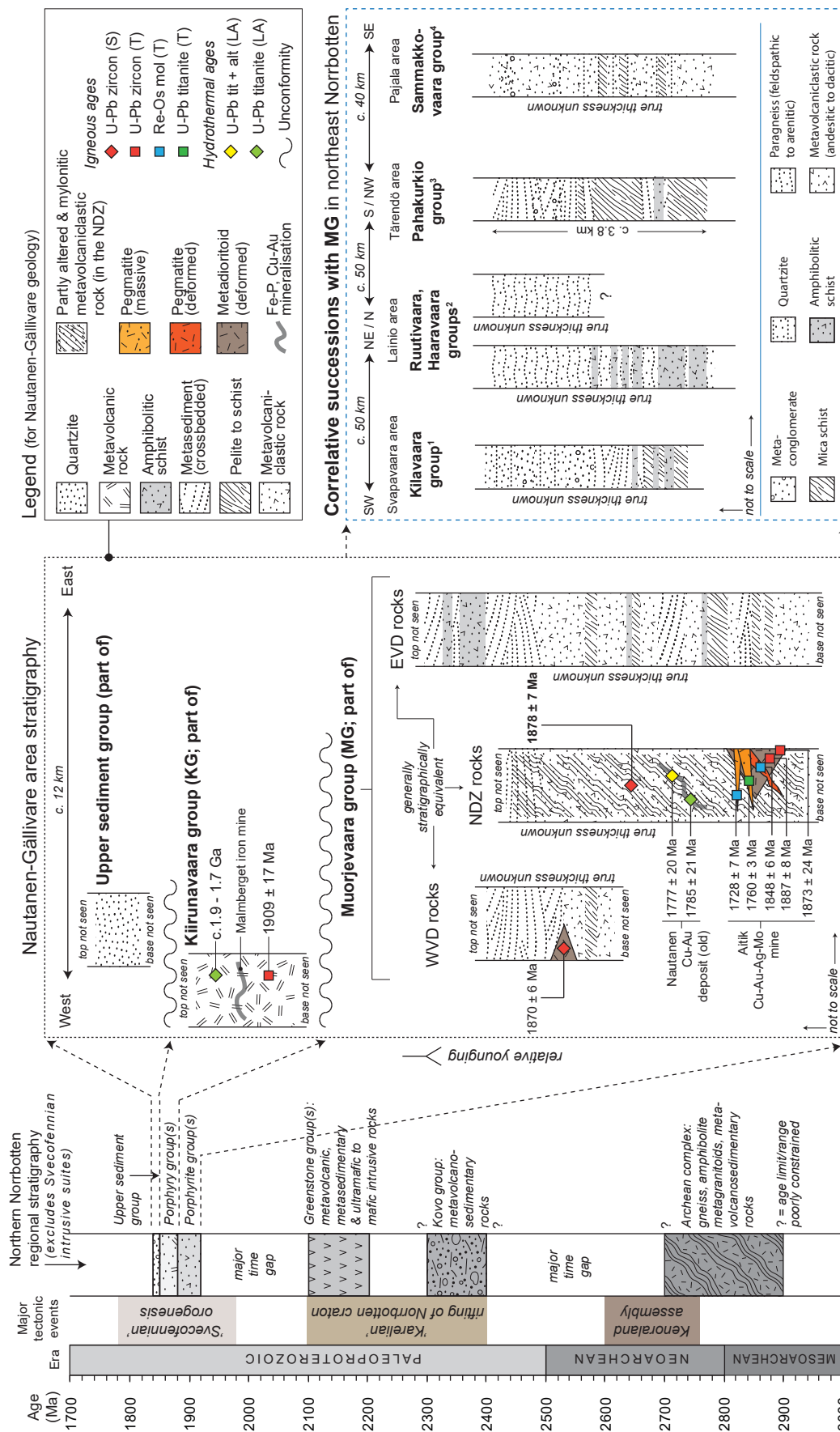


Figure 3. Outline stratigraphy of northern Norrbotten and the Gällivare area (based on descriptions by Witschard 1996, Bergman et al. 2001 and Martinsson & Wanhaien 2004). Abbreviations: EVD = eastern volcanosedimentary domain, KG = Kirunavaara group, MG = Muorjevaara group, NDZ = Nautanen deformation zone domain, WVD = western volcanosedimentary domain. Geochronology abbreviations and sources: U-Pb SIMS (S) zircon ages = Sarius 2016, and this study (bold text); U-Pb TIMS (T) zircon ages = Skiöld & Cliff (1984), Wanhaien et al. (2006); Re-Os TIMS (T) molybdenite (mol) ages = Wanhaien et al. (2005); U-Pb TIMS (T) and laser ablation mass spectrometry (LA) titanite (tit) and allanite (alt) ages = Wanhaien et al. (2005), Storey et al. (2007), Smith et al. (2009). Schematic stratigraphy of correlative northeast Norrbotten successions is based on: 1 = Eriksson and Hallgren 1975; 2 = Witschard 1970; 3 = Padgett 1970, 1977; 4 = Martinsson 2004.

NDZ (e.g. Nautanen deposit, Danielsson 1985); and (2) mineralisation associated with quartz \pm tourmaline \pm amphibole veins occurring mainly east of the NDZ (e.g. Ferrum prospect, Gustafsson & Johnsson 1984), or as a late-stage brittle overprint within the high-strain zone (e.g. at the Nautanen deposit).

The area around the Nautanen deposit in the northern NDZ domain is a historical mining location that has experienced intermittent exploration for over 100 years. Copper mineralisation was first discovered in 1898, and approximately 72 000 tonnes of copper and iron ore were extracted between 1902 and 1907 (Geijer 1918). Gold was not mined at that time, however. Further exploration in the 1970s and 80s produced a pre-regulatory total resource estimate for the “old” Nautanen deposit of approximately 2.94 Mt grading 0.78% Cu and 0.52 ppm Au (values derived from Danielsson 1985). Present-day exploration has resulted in the discovery of additional Cu-Au mineralisation approximately 1.6 km north-northwest of the old Nautanen mine along the trend of the NDZ (Fig. 2). This “Nautanen North” deposit has an indicated resource of 9.6 Mt grading 1.7% Cu, 0.8 ppm Au, 5.5 ppm Ag and 73 ppm Mo, with an additional inferred resource of 6.4 Mt grading 1.0% Cu, 0.4 ppm Au, 4.6 ppm Ag and 41 ppm Mo (New Boliden 2016).

According to criteria presented by Grooves et al. (2010), the geological characteristics of the Nautanen Cu-Au deposit are consistent with the restricted definition of a *bona fide* iron oxide-copper-gold (IOCG) system. These include (1) enrichment of Cu and Au, with both elements representing potential economic commodities; (2) a spatial and genetic association between the mineralisation and iron silicate and iron oxide gangue minerals (i.e. *not* an iron oxide or iron oxide-apatite deposit with anomalous Cu and Au; cf. Williams 2010); (3) hydrothermal mineralisation style (i.e. replacement lenses, zones and veins); (4) sulphur mainly present in the S²⁻ oxidation state; (5) clear structural controls on the mineralisation; and (6) a temporal association with magmatism and deformation, but no obvious causative intrusion.

Pervasive and vein-related potassic-ferroan \pm calcic alteration occurs variably in the NDZ domain and adjacent areas, and is associated with IOCG and related mineralisation (cf. McGimpsey 2010, Lynch et al. 2015; see also *Lithological characteristics* section). At the “old” Nautanen deposit (Fig. 2), characteristic almandine porphyroblasts are associated with amphibole + biotite + magnetite + sericite \pm K-feldspar \pm sulphide and tourmaline \pm quartz \pm sulphide banding, patches and veins (Fig. 4A–D). Textural relationships suggest garnet growth slightly predates the main-stage alteration and mineralisation event (cf. Waara 2015). Late-stage epidote \pm quartz \pm carbonate alteration also occurs (Fig. 4B–C). Chalcopyrite with lesser bornite and chalcocite are the main Cu-bearing minerals and are typically associated with pyrite, pyrrhotite, magnetite and tourmaline (Fig. 4D–E). Quartz-amphibole \pm tourmaline veins containing pyrite and minor chalcopyrite post-date the main-stage disseminated and microfracture type sulphide mineralisation (e.g. Fig. 4F). Gold generally occurs as inclusions and segregations in pyrite, chalcopyrite, Bi-bearing phases and locally galena (e.g. Sammelin 2011, Bark et al. 2013).

At deformation zone- or belt-scale, particularly with respect to the NDZ, metal enrichment and depletion patterns are evident, reflecting bulk geochemical mobility in the area (Tollefsen 2014, Lynch et al. 2015). For example, comparison of “least altered” meta-volcanosedimentary rocks from the eastern volcanosedimentary domain with NDZ-hosted samples (pervasively altered, mylonitic) shows that the latter are relatively enriched in Cu, Ag, Au, Fe, Mo, Ba, Mn and W. Likewise, the tendency for K/Na ratios to increase when stepping into the NDZ domain reflects the association between potassic alteration and Cu-Au-Fe enrichment (cf. Lynch et al. 2015). These features are diagnostic of typical geochemical affinities and metal abundance correlations associated with IOCG-style mineralisation, particularly deposits hosted by intermediate to felsic igneous rocks in continental settings (cf. Barton 2014).

Smith et al. (2009) reported U-Pb LA-ICP-MS titanite and allanite ages ranging from c. 1.79 to 1.78 Ga for hydrothermal alteration at the Nautanen Cu-Au deposit (cf. Figs. 2 & 3). These dates provide a temporal and inferred genetic link between the mineralisation and deformation, fluid mobilisa-

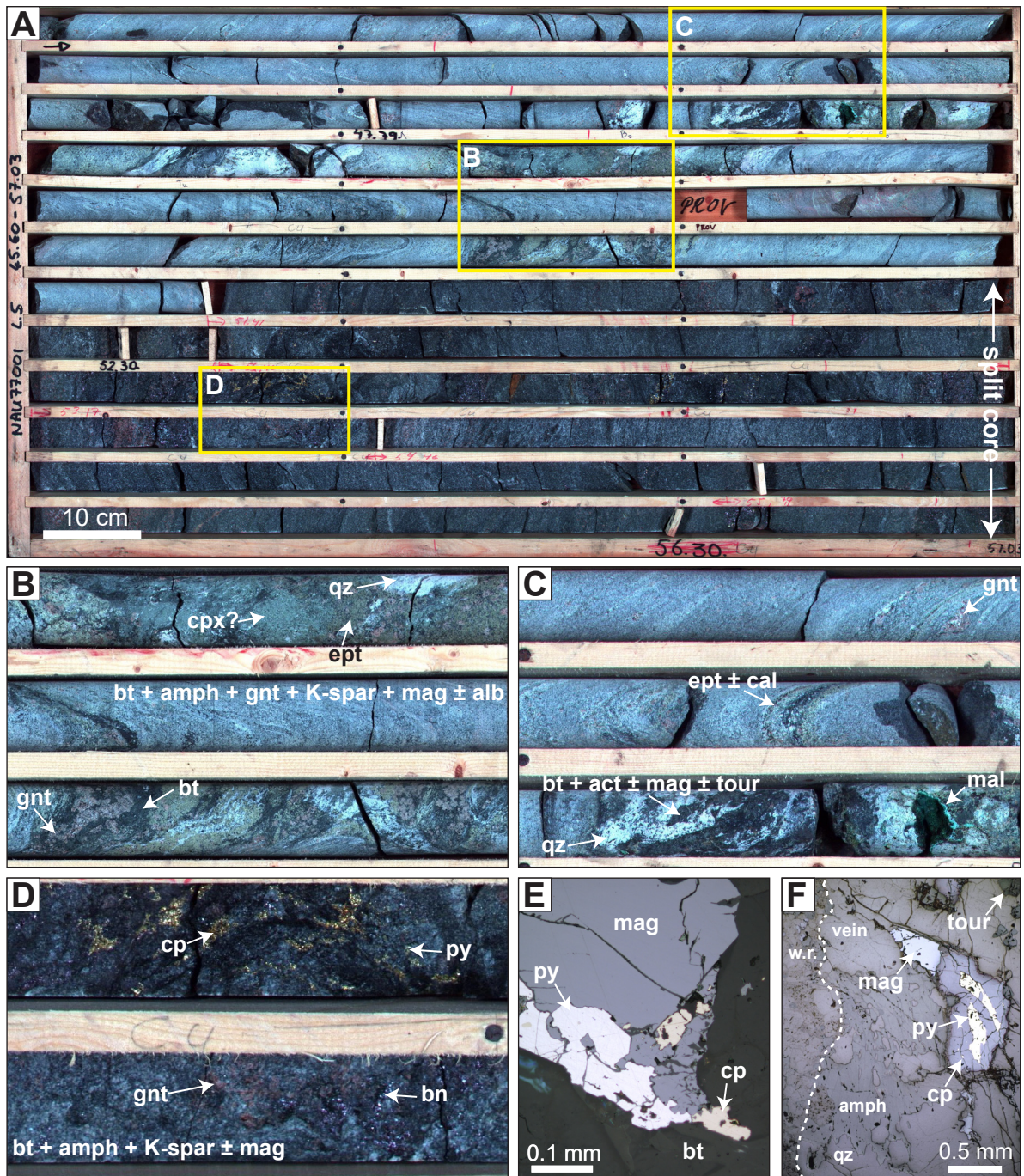


Figure 4. Alteration and mineralisation characteristics of the Nautanen IOCG deposit. **A.** True-colour image of an approximately 11.4 m section of altered and mineralised drill core (drill hole NAU77001). The lower six rungs contain split core. **B.** Foliated biotite-amphibole schist showing patchy and vein style, moderate to intense, biotite + garnet + K-feldspar \pm albite \pm magnetite alteration. A late-stage epidote \pm calcite assemblage is also present. **C.** Foliated biotite-amphibole schist with disseminated garnet porphyroblasts associated with a possible early sodic-calcic (albite + scapolite) alteration (top rung). Some thin epidote + calcite veinlets also occur. The lower rung contains a replacement zone of biotite + chalcopyrite + bornite \pm magnetite \pm tourmaline and late-stage carbonate. **D.** Disseminated and irregular patches of chalcopyrite + pyrite + bornite associated with biotite + amphibole + garnet \pm K-feldspar \pm magnetite alteration. **E.** Thin section reflected light (RL) view of disseminated chalcopyrite and pyrite associated with magnetite. **F.** Thin section RL view of a quartz-amphibole-tourmaline vein containing pyrite, magnetite and rare chalcopyrite. W.r. = wall rock. Mineral abbreviations: act = actinolite, alb = albite, amph = amphibole, bn = bornite, bt = biotite, cal = calcite, cp = chalcopyrite, cpx = clinopyroxene, ept = epidote, gnt = garnet, K-spar = K-feldspar, mag = magnetite, mal = malachite, py = pyrite, qz = quartz, tour = tourmaline.

tion and late-orogenic granitic magmatism (cf. Fig. 3). Given the protracted and episodic nature of magmatic-hydrothermal processes and Cu-Au mineralisation at the Aitik deposit, south of Nautanen (e.g. Wanhainen et al. 2005), it is likely that coupled deformation-hydrothermal processes within the NDZ may have been active over a similarly protracted period.

Lithological characteristics of Muorjevaara group rocks

Petrographic descriptions presented in this section complement previous accounts by Zweifel (1976), Ros (1980), Monro (1988) and Lynch et al. (2015).

In general, four lithological units are recognised. They are (1) predominantly intermediate metavolcaniclastic rocks; (2) volcanogenic (epiclastic) metasedimentary rocks; (3) mica schist horizons; and (4) amphibolitic schist (mafic metavolcaniclastic rocks). Units 1 and 2 are the most common units across the Nautanen area.

Units 1, 2 and 3 represent compositionally similar lithologies (mainly basaltic andesitic to andesitic) and are primarily distinguished on the basis of textural, structural and deformation intensity criteria. In the Nautanen deformation zone domain, deformed and altered feldspar-biotite-amphibole schist (locally gneiss) is inferred to represent a composite intermediate metavolcaniclastic unit, probably consisting of a combination of units 1 to 3 (unit no. 5, Table 1).

Intermediate metavolcaniclastic rocks

In the central eastern volcanosedimentary domain, the predominant rock type is a medium to dark grey, fine- to medium-grained (approximately 0.1–3 mm), laminated and locally compositionally banded, metavolcaniclastic rock (Fig. 5). It forms planar to weakly wavy, generally sub-parallel, medium to very thick (approximately 0.1 to 1 m), laterally continuous beds (Fig. 5A–B). Inter-bed contacts are narrowly gradational to sharp. Internal textural and compositional consistency is somewhat variable and includes generally homogenous, well-sorted and granular units (fine to coarse tuff), and banded, layered and laminated sequences (Fig. 5C–E). Locally, the tuffaceous granular sections grade into somewhat irregular and wavy weathering beds consisting of mica-rich schist or relatively coarse (approximately 1–4 mm), feldspathic-rich bands and seams (Fig. 5B; cf. Fig. 7). The former tend to have a strongly developed micaceous sheen, whereas the latter may in part represent more compositionally felsic horizons or aplitic veins. Locally, tuffaceous sections display multiple, repeat grading sequences that alternate between very coarse tuff at the base (sometimes containing somewhat pumaceous, felsic clasts, Fig. 5F) to fine tuff at the top (thus, possible reverse density grading?, Fig. 5E). In addition, local horizons display cross-laminae that indicate general younging towards the southwest (Fig. 5F).

► Figure 5. Metavolcaniclastic rocks in the Nautanen area. **A.** Along-strike view (to the south-east) of medium- to thickly-bedded, intermediate, fine to coarse tuff. **B.** Bedding view to the southwest of thin- to medium-bedded, compositionally and texturally banded, intermediate metavolcaniclastic rock. **C.** View to the east-southeast of recrystallised, intermediate fine to coarse tuff. **D.** View to the northeast of intermediate metavolcaniclastic unit (tuff) with steeply dipping, sub-parallel amphibole-magnetite veinlets. **E.** Bedding view (to the northeast) of thinly laminated, well-sorted, fine to coarse tuff. Slightly coarser, epidote-altered, layers (arrows) with rare sub-rounded clasts indicate possible normal grading to the NE. **F.** Bedding view (to the southwest) of finely laminated, well-sorted, intermediate tuff with remnant elongate (feldspathic) clast. Broken lines indicate orientation of laminae (cross-lamination), indicating younging direction. **G.** Bedding view (to the southwest) of variably biotite-magnetite-altered and schistose, fine to coarse, lithic tuff. Two types of deformed clasts are visible; aggregated granular clasts (dashed outline), and relatively homogenous felsic clasts (arrows). **H.** Bedding view (to the west-southwest) of poorly sorted and foliated volcanoclastic (agglomeritic) unit, containing a mixture of deformed, angular to sub-rounded coarse (lapilli and block-sized) granular (intrusive?) and fine-grained felsic clasts. All photographs by Edward Lynch.



The metavolcaniclastic rock mainly consists of feldspar, amphibole, biotite and minor quartz and muscovite within a fine-grained, intergranular (granoblastic) to foliated (lepidoblastic) matrix. Feldspar is anhedral, tabular to sub-rounded (platy) and is generally sericitised. Locally, feldspar also forms remnant, medium-grained (approximately 3–5 mm) phenocrysts (approximately 5–8 vol. %). Anhedral prismatic amphibole (hornblende) is intergrown with biotite and feldspar as irregular, matted, elongate and cleaved grains. Local magnetite disseminations or thin bands and veinlets (<1 cm) occur, and prismatic and tabular grains tend to exhibit a preferred sub-parallel alignment (generally parallel to primary structures and foliations). Generally, biotite and feldspar occur in approximately equal proportions (approximately 30–45 vol. %). However, biotite ± sericite are locally predominant (up to approximately 60–70 vol. %), thus imparting a more obvious mica schist appearance to the rock (see unit 3 below). These latter intercalations may represent more altered horizons.

Locally, metavolcaniclastic sections contain coarser clastic material (>3 mm) forming fine- to medium-grained lapilli-tuff horizons. In addition, poorly-sorted sections containing coarse, blocky clasts form local agglomeritic (volcanic breccia-like) horizons (Fig. 5G–H). Two broad clast types are recognised: fine-grained (<0.5 mm), sub-rounded to elongate or flattened, compositionally uniform felsic clasts (possible juvenile volcanic clasts, Fig. 5G), and medium to coarse (approximately 0.1–10 cm), aggregated granular types (probably lithic clasts, Fig. 5H). In poorly-sorted sections, the latter clasts are locally up to 8 cm in size (Fig. 5H).

Overall, metavolcaniclastic rocks display a degree of compositional and textural variability across the sequence that reflects the generally interbedded nature of the eastern volcanosedimentary domain and the magnetic anomaly patterns across the area.

Volcanogenic (epiclastic) metasedimentary rocks

Throughout the eastern volcanosedimentary domain, interbedded sections of medium-grey, well-sorted, fine- to medium-grained (approximately 0.1–3 mm), generally arkosic metasedimentary rocks occur (Fig. 6). Locally, the interbedded sections transition into relatively thick sequences (approximately 500–800 m apparent thickness).

In the Muorjevaara area (northern part of the eastern volcanosedimentary domain, Fig. 2), a relatively well-exposed approximately 150 m long stratified metasedimentary sequence occurs (Fig. 6A). Here, the rocks form planar, parallel to locally non-parallel, thin to thick (approximately 0.03–0.4 m) and generally laterally continuous beds (Fig. 6A–D). Inter-bed contacts are either narrow diffuse (over approximately 0.1 m) or distinctive and sharp (e.g. Fig. 6C). Internally, the beds contain planar to locally wavy, generally parallel and laterally continuous, thin to medium (approximately 0.1–0.3 cm) laminae. Locally, however, parallel and lenticular non-parallel beds exhibit inclined cross-laminae (tabular to trough-style, respectively, Fig. 6E–F). Local co-sets display bi-directional, herringbone-type cross-lamination (Fig. 6F). In general, topset laminae and bedding contacts truncate low-angle ripple foresets towards the southwest, constraining way-up and younging direction. Likewise, in the central and southeastern volcanosedimentary domain, on the eastern limb of a large synform, cross-stratification suggests general younging towards the southwest (i.e. towards the hinge zone of the fold). These way-up indicators are locally supported by rare, normal-graded sequences (Fig. 6C). Ripple foreset patterns indicate paleocurrent directions mainly towards the north-northwest, or occasionally towards the south-southeast, while in general the cross-bedding structures suggest an above wave-base, sub-aqueous depositional setting.

At outcrop scale, metasedimentary rocks appear relatively homogenous and more lithologically consistent than other volcaniclastic and schistose sections, consisting of intergranular (granoblastic) feldspar and quartz with minor amphibole and rare muscovite. Locally, some beds are affected by patchy to banded biotite + amphibole + magnetite and epidote ± carbonate alteration. The latter assemblage is generally more prevalent and appears to preferentially overprint coarser (coarse to very coarse

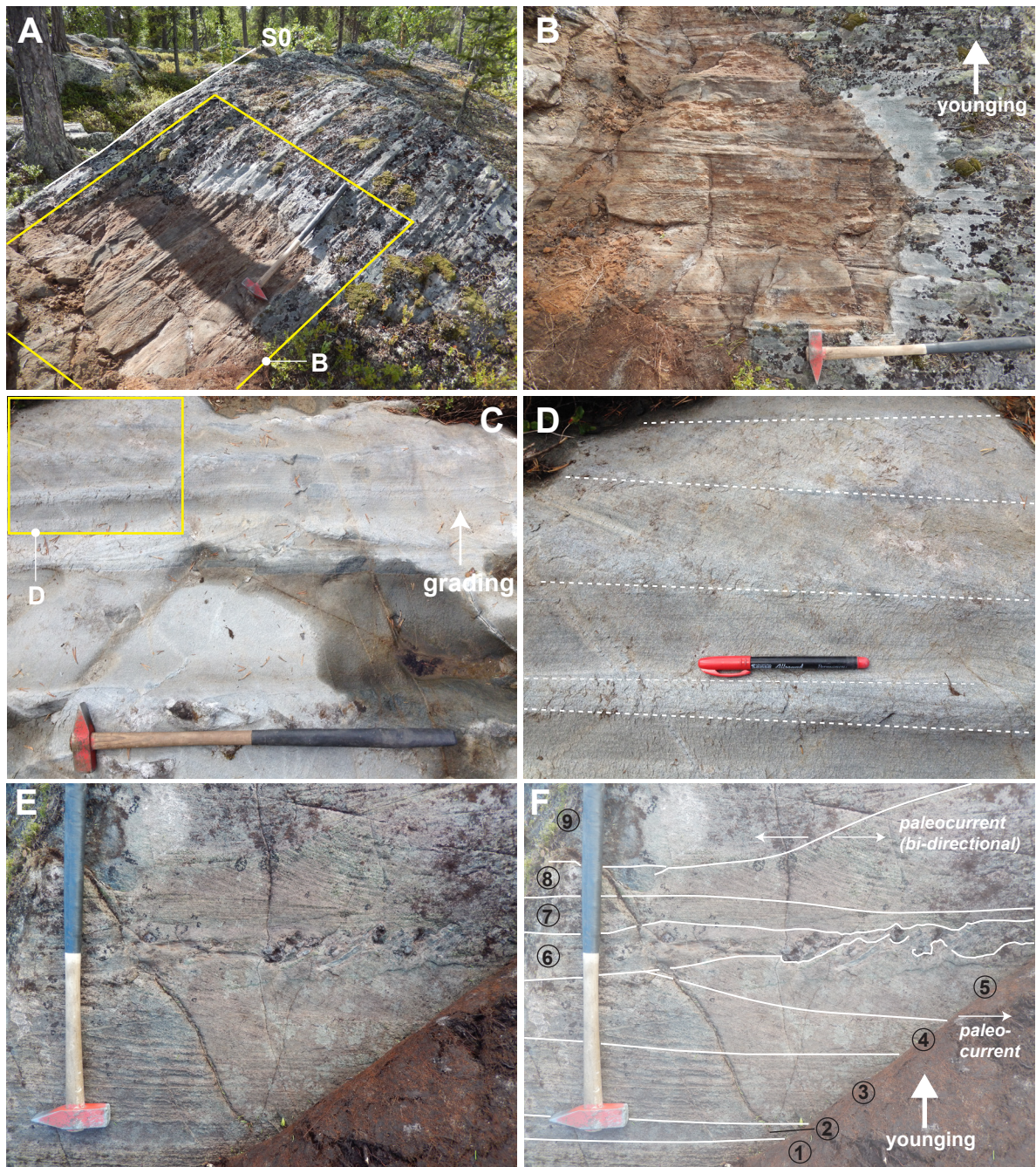


Figure 6. Volcanogenic (epiclastic) metasedimentary rocks in the Nautanen area. **A.** View to the west of planar, sub-parallel and laterally continuous, thin- to medium-bedded, arkosic metasedimentary rock (volcanic siltstone to sandstone). **B.** Detail from A with younging direction towards the southwest. **C.** Bedding view (to the southwest) of fine-grained, medium- to thickly-bedded metasedimentary rock. **D.** Detail from C showing sub-parallel, planar beds. **E.** Bedding view (to the southwest) of thin- to thickly-bedded, planar to curved (non-parallel) metasedimentary rock. **F.** Interpretive sketch of E showing nine bedding co-sets. Sets 4, 5, 8 and 9 contain inclined (ripple) foresets, indicating low-angle trough cross-lamination (sets 4 and 5) and herringbone cross-lamination (sets 8 and 9). All photographs by Edward Lynch.

sand) horizons. In general, a typical stratified sequence (approximately 0.5–2 m thick) consists of alternating very fine to coarse sand (approximately 0.1–1 mm) within planar and parallel laminated beds (Fig. 6C–F). These grade locally into wavy and cross-laminated horizons, more typically consisting of coarse to very coarse sand (approximately 1–2 mm) These general depositional characteristics are

relatively consistent with medium-grained turbidite sequences (cf. Tucker 1991). Other minor features within rocks include siliceous, sub-rounded concretions (approximately 3–5 cm) locally developed at bedding contacts, and amphibole, epidote and quartz veins.

In general, the observed sedimentary structures are consistent with a sub-aqueous depositional environment. The preserved cross-bedding and herringbone-type cross laminae suggest above-wave-base or intertidal depositional environments. In terms of source material provenance and processes, the metasedimentary rocks probably represent either volcanoclastic material re-deposited within an active volcanosedimentary basin (i.e. syn-eruptive redeposition as defined by McPhie et al. 1993), primary unconsolidated volcanoclastic material, redeposited during volcanically quiescent periods (“immature” epiclastic rocks described by Cas & Wright (1988), or equate to the volcanogenic sedimentary deposits of McPhie et al. 1993). Older, detrital material (volcanic ± plutonic) most likely also contributed source material. Further petrographic and geochemical evidence for a predominantly volcanogenic source of the metasedimentary rocks includes the interbedded and gradational nature of this unit with other metavolcanoclastic rocks, the abundance of plagioclase feldspar in the matrix, and its general intermediate (andesitic) geochemical composition, similar to the metavolcanoclastic units within the sequence (see *Lithochemistry* section).

Pelite or mica schist

Intercalations of mica schist occur locally throughout the main meta-volcanosedimentary package and are preserved in both the eastern and western volcanosedimentary domains (Fig. 7). They typically form approximately 0.3 to 1.5 m thick, planar to laterally dilational units, with generally narrow, gradational contacts. At outcrop scale, they are recognised as texturally distinctive horizons that typically exhibit a more micaceous (lustrous), weathering-proud and schistose appearance than more granoblastic and recrystallised metavolcanoclastic and metasedimentary rocks. Locally, cross-bedding or climbing ripple-type structures are preserved, suggesting clastic depositional processes (Fig. 7A). Other horizons have a laminated, pelitic appearance (Fig. 7B). Metamorphic or fabric intensity ranges from phyllitic to schistose types, with the latter consisting of thinly spaced (approximately 0.5–2 mm), compositionally variable (mesocratic-melanocratic) banding (Fig. 7C). This textural variation probably reflects local contrasts in grain size, deformation intensity, mineralogy and composition, and somewhat mimics the broader lithological variability seen throughout the meta-volcanosedimentary sequence.

Mica schist horizons consist of fine-grained (<1 mm), intergranular biotite and feldspar, with lesser muscovite, amphibole and quartz (Fig. 7A–B). Mica grains are aligned and flattened parallel to the main schistosity and sub-parallel to inferred bedding, while medium-grained (approximately 3–5 mm) garnet porphyroblasts also occur locally (Fig. 7B). Typically, where garnet and andalusite occur, secondary hematite-goethite is exposed on weathered surfaces. Pervasive, weak to moderately intense sericite weathering is locally developed. Thin seams and veinlets of feldspathic material are also locally developed, are typically orientated parallel to the main schistosity, and are sometimes tightly folded.

Amphibolite schist (mafic metavolcanoclastic rock)

A prominent amphibolitic schist unit occurs in the southeastern volcanosedimentary domain (river Linaälven area) within the hinge zone of a major S-SE-plunging synform (Fig. 7D–F). The rock is dark grey to dark greenish-grey and is generally aphanitic to locally amphibole-porphyrific (approximately 3–7 vol. % phenocrysts). It consists of medium- to coarse-grained (approximately 1–8 mm), generally sub-rounded, anhedral platy to elongate (subhedral prismatic) amphibole (approximately 40–50 vol. %) within a fine-grained (<1 mm), plagioclase-amphibole-biotite ± magnetite matrix (approximately 35–45%). Recrystallisation of plagioclase and secondary phases such as biotite and chlorite (replacing amphibole) are common. Locally, scapolite appears to replace plagioclase.



Figure 7. Lesser intercalated rock units in the Nautanen area. **A.** View to the west-southwest of mica schist with possible cross-bedding structures. The pencil is about 15 cm long. **B.** Sub-horizontal surface view to the east-northeast of mica schist with garnet porphyroblasts. The pencil is 1 cm wide. **C.** Sub-horizontal surface view to the southwest of muscovite schist unit with a wavy and strongly foliated texture. **D.** Sub-vertical surface view to the north-northwest of amphibole-feldspar schist. **E.** Sub-horizontal surface view to the west-northwest of amphibolite schist near the river Linaälven, containing elongate or stretched lithic clasts (arrows). **F.** Sub-horizontal surface view to the east-southeast of foliated amphibolitic schist with weakly developed dextral shear planes. All photographs by Edward Lynch, except D by Zmar Sarlus.

The rock has a relatively intense deformation fabric, which imparts an overall schistose appearance (Fig. 7D). The schistosity is typically sub-vertical, north-northwest-orientated and steeply dipping. Weakly developed asymmetric shear bands also occur and suggest dextral oblique movements (Fig. 7F). Locally, thin feldspathic lenses and veinlets occur, sub-parallel to the main fabric. Additionally, elon-

gate and stretched clasts are present. These display mainly remnant igneous (dioritic) textures (Fig. 7E). Clasts are typically aligned parallel to the main fabric in the rock (Fig. 7E).

Analogous amphibolitic units occur locally throughout the study area as fairly thin (<1 m) intercalations within the main metavolcaniclastic package. Similar rocks have been observed in the central part of the Nautanen deformation zone and at the Salmijärvi Cu-Au prospect, approximately 2 km south-southeast of the Aitik mine (Sarlus 2013).

Biotite-amphibole schist to gneiss (Nautanen deformation zone)

The bedrock in the Nautanen deformation zone (NDZ) domain is affected by relatively intense shearing, transposition and metasomatic-hydrothermal alteration (Fig. 8). Thus, primary lithological characteristics are commonly obscured or masked by overprinting processes and remain somewhat equivocal (cf. Witschard 1996). Nevertheless, local low-strain and “least altered” zones provide some petrographic insights into the primary nature of the rocks in this area and facilitate comparisons with the rocks in the other two lithological-structural domains.

The predominant lithology is a medium to dark grey, fine- to medium-grained (approximately 0.1–3 mm), well-sorted and internally laminated, feldspar-biotite ± amphibole schist to gneiss (Fig. 8A). Locally, more weakly laminated varieties have a recrystallised, granoblastic appearance and appear more feldspar-rich (up to approximately 40 to 50 vol. %). Inferred bed forms (although rarely preserved) are approximately 0.1–0.5 m thick and are generally laterally continuous, sub-parallel and planar. In general, anhedral and platy biotite and lesser amphibole grains (approximately 15–20 and 5–10 vol. %, respectively) are aligned parallel to the dominant penetrative cleavage and intergrown with feldspar. Local horizons containing coarser (felsic) clasts (approximately 5–15 mm), elongate and stretched lensoidal patches (remnant clasts?), and composite, aggregated fragments (lithic clasts?) occur throughout the area. These features are consistent with a possible volcaniclastic derivation (cf. Fig. 5G–H). Locally, the schist grades into more quartz-rich sections consisting of fine-grained (<1 mm), granular and anhedral quartz (approximately 10–20 vol. %), forming banded zones and aggregated, irregular to sub-rounded, lithic (?) clasts.

Throughout the Nautanen deformation zone domain the bedrock displays moderate to intense penetrative foliation and shows variable degrees of metasomatic-hydrothermal alteration (see *Structural geology and deformation* section). Distinctive dark red to pinkish-red, medium- to coarse-grained (typically approximately 1–10 mm) garnet porphyroblasts occur locally (approximately 3–12 vol. %). These appear to pre-date the main alteration assemblage and copper mineralisation event (Fig. 8C–D, e.g. Waara 2015). Locally, the garnets form quite large crystals up to 10 cm in diameter or aggregated clusters (cf. Fig. 13C). The garnets are typically of the spessartine-almandine variety, appear to be mainly syn-kinematic, and form disseminated grains or clusters associated with amphibole + biotite + magnetite veins and patches (Fig. 8C–D). Waara (2015) has suggested a link between garnet growth and early stage IOCG-related alteration, and constrained their formation at approximately 630–680°C by Thermocalc modelling.

The most important belt- to deposit-scale alteration assemblage affecting Nautanen deformation zone rocks is a moderate to intense amphibole + biotite + K-feldspar + magnetite ± garnet ± sericite ± pyrite ± chalcopyrite assemblage. Typically, it has developed along seams, linear zones and irregular veins trending parallel to the transposed foliation (Fig. 8B–C). This inferred “syn-mineralisation” assemblage overprints an earlier pervasive scapolite ± albite assemblage (Fig. 8B). Zones and bands of tourmaline ± quartz alteration represent a paragenetically later assemblage.

Syn-mineralisation magnetite typically occurs as fine- to medium-grained (approximately 0.1–2 mm), anhedral tabular and elongate platy grains within foliation planes. It also forms fracture-filling inclusions and patchy rims around garnet porphyroblasts. Consequently, the bedrock throughout the domain is magnetically anomalous (cf. Fig. 14; see *Structural geology and deformation* section). Locally,

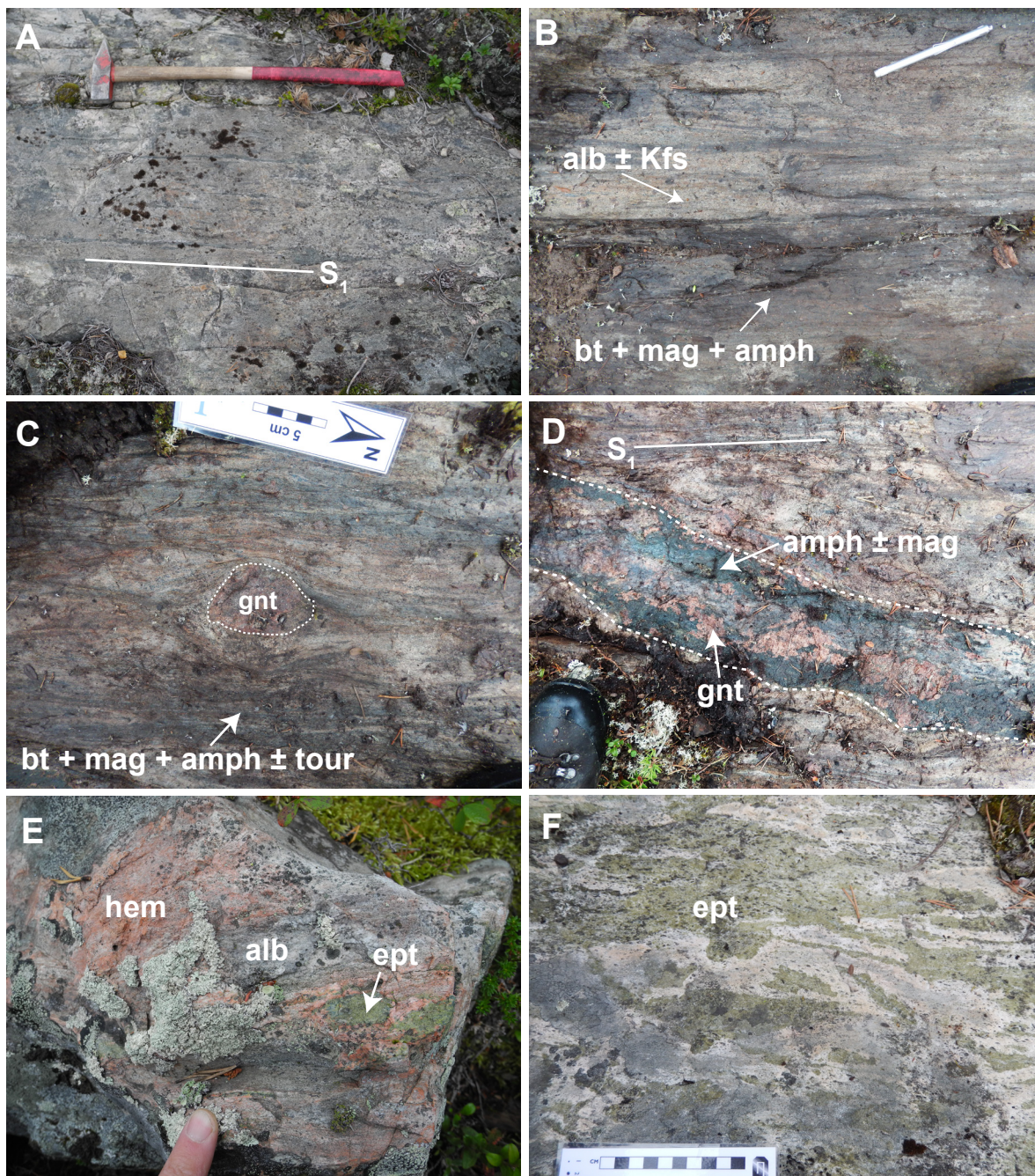


Figure 8. Variably altered biotite-amphibole-feldspar schist in the Nautanen deformation zone (inferred metavolcaniclastic unit). **A.** Relatively weakly altered. **B.** Banded metavolcaniclastic rock. **C.** Moderate to intensely altered rock. **D.** Moderate to intensely altered rock cut by an amphibole-garnet zone or vein. **E.** Feldspar-rich metavolcaniclastic rock showing pervasive “red rock” type hematite staining of feldspar (cf. Carlon 2000). Late-stage patchy epidote also developed. **F.** Late-stage epidote alteration of metavolcaniclastic rock. Abbreviations: alb = albite, amph = amphibole, bt = biotite, ept = epidote, gnt = garnet, hem = hematite, Kfs = K-feldspar, mag = magnetite, tour = tourmaline. All photographs by Edward Lynch.

feldspar-rich metavolcaniclastic rocks display reddish-pink patches and irregular zones indicative of “red rock”-type hematite staining and iron exsolution affecting alkali feldspar (Fig. 8E; cf. Carlon 2000). A late-stage epidote \pm quartz \pm carbonate alteration assemblage is also present and more typically overprints red rock (K-feldspar-altered) zones (Fig. 8E–F). Secondary hematite-goethite commonly replaces magnetite, while chlorite replaces biotite and is associated with epidote.

Lithochemistry of Muorjevaara group rocks

Preliminary lithochemistry results for meta-volcanosedimentary rocks from the eastern volcanosedimentary domain (EVD) are shown in Figure 9. Although the Nautanen area is affected by varying degrees of hydrothermal alteration (see above section), rocks in the EVD are generally less pervasively altered than those in the Nautanen deformation zone domain. Likewise, the inferred metamorphic grade (mid to upper greenschist facies) in the EVD is lower than that in the Nautanen deformation zone (cf. Bergman et al. 2001).

From a total of 32 analyses, a subset ($n=24$) of relatively fresh or “least altered” eastern volcanosedimentary domain samples were selected to geochemically characterise the meta-volcanosedimentary rocks (Fig. 9A, shaded area). The subset includes scapolite + albite + sericite-altered samples of fine- to medium-grained, plagioclase-phyric, metavolcaniclastic rock with an elevated Na_2O concentration of approximately 7 wt. %.

Based on the classification plot of Winchester & Floyd (1977), least altered EVD meta-volcanosedimentary rocks generally have a basaltic andesitic to andesitic signature (Fig. 9B), while high-field strength element bivariate plots indicate a predominantly calc-alkaline composition (Fig. 9C–D). Metavolcaniclastic, meta-epiclastic, mica schist and amphibolitic schist samples have similar calc-alkaline, intermediate compositions, suggesting a possibly similar volcanic provenance and petrogenetic history. The altered feldspar-phyric metavolcaniclastic sample plots close to the andesite-dacite boundary and has broadly similar trace element systematics to the other samples (Fig. 9A–B).

The geochemical signatures of the meta-volcanosedimentary rocks from the eastern volcanosedimentary domain partly overlap the compositions of altered and mylonitic metavolcaniclastic rocks in the Nautanen deformation zone domain hosting the Nautanen Cu-Au deposit (Fig. 9B; cf. McGimpsey 2010). The latter units have a broader compositional range that includes dacitic, rhyodacitic and trachyandesitic (shoshonitic) varieties. However, the presence of (apparently) alkaline rocks within the Nautanen deformation zone domain may partly reflect a higher degree of potassic \pm sodic alteration and “skarn” banding there (cf. Fig. 8B–C). Similar apparent alkaline enrichment is reported for metavolcaniclastic rocks hosting the Aitik Cu-Au-Ag deposit (Monro 1988, McGimpsey 2010), which also compositionally overlap both the eastern volcanosedimentary domain and Nautanen deformation zone domain metasedimentary rocks (Fig. 9B).

Overall, the preliminary lithochemistry results confirm that NDZ domain rocks represent a more intensely deformed and hydrothermally altered variety of the units occurring in the eastern domain, and that the Muorjevaara group sequence in the Nautanen area is compositionally similar to the metavolcaniclastic rocks (biotite-amphibole-feldspar gneiss) hosting Cu-Ag-Au mineralisation at Aitik (cf. Monro 1988, Martinsson & Wanhainen 2004).

The lithochemistry results support lithostratigraphic correlations between Muorjevaara group rocks in the Nautanen area and meta-volcanosedimentary successions in northeastern Norrbotten (Pajala shear zone). For example, Luth et al. (2015) report sub-alkaline, mainly andesitic to rhyodacitic compositions for metavolcanic and metavolcaniclastic rocks assigned to the *Suorsa group* in the Pajala area. Certain units within this local group may be equivalent to the *Pahakurkio* and *Sammakovaara groups* in adjacent areas and are inferred to belong to the regional Porphyrite group of Bergman et al. (2001).

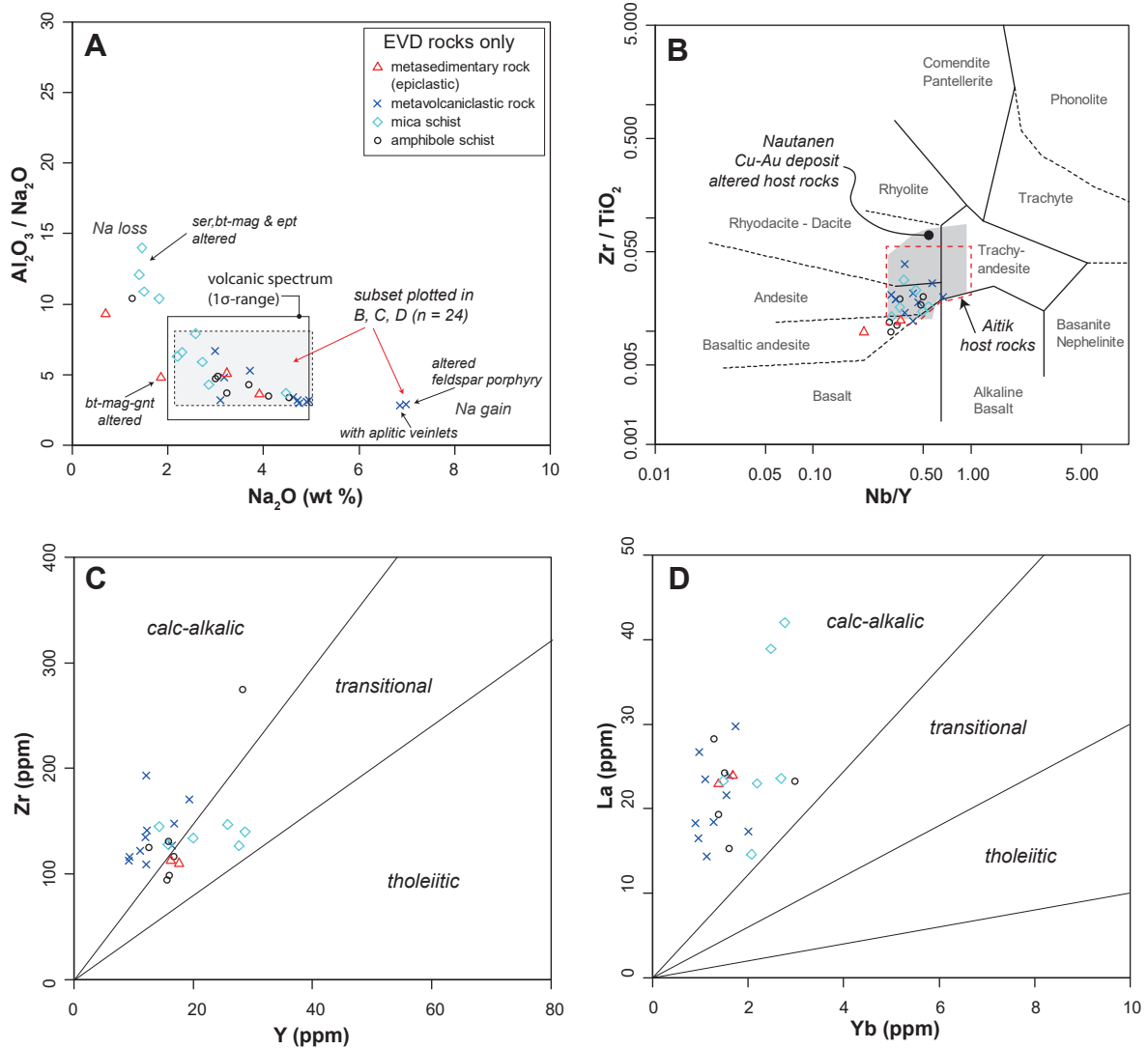


Figure 9. Geochemical classification of Muorjevaara Group meta-volcanosedimentary rocks from the EVD, Nautanen area. **A**. Spitz-Darling type plot (Spitz & Darling 1978), delineating weakly altered samples used for the other classification plots shown in B, C and D. The spectrum for fresh volcanic rocks (basalt to rhyolite) is derived from the average and 1 σ -range of 6 491 analyses reported by Le Maitre (1976). **B**. Incompatible-HFSE classification plot (Winchester & Floyd 1977) showing lithologic-compositional range of EVD meta-volcanosedimentary rocks. The shaded area represents the range reported by McGimpsey (2010) for altered metavolcaniclastic rocks hosting the Nautanen Cu-Au deposit. The broken red line represents the approximate range for metavolcaniclastic rocks hosting the Aitik Cu-Au-Ag deposit (cf. Monro 1988). **C–D**. Incompatible-HFSE bivariate plots (Barrett & MacClean 1999), indicating a predominantly calc-alkalic signature (i.e. equivalent to medium to high K, low to medium Fe, intermediate rocks).

Summary of Muorjevaara group rock units

A summary of Muorjevaara group lithologies is presented in Table 1. It includes a comparison between historical terms used for each unit and the field and protolith terms derived from this study.

Table 1: Outline description of Muorjevaara group rock units

Field term (with textural or metamorphic qualifiers, and inter-unit relationships)	Protolith term (with textural or compositional qualifiers) ¹	Historical, literature term (with reference)
<i>In the eastern and western volcanosedimentary domains (Fig. 2)</i>		
1. Metavolcaniclastic rock (tuffaceous, recrystallised, locally schistose; local volcanic and lithic clasts; compositionally banded, laminated; transitional or interbedded with 2, 3 and 4)	Andesitic to dacitic (intermediate), well-sorted, fine to very coarse tuff, to lapilli-tuff. Locally poorly sorted lithic tuff with agglomeritic (volcanic breccia) horizons.	Leptite (Geijer 1918) Biotite gneiss (Ros 1980) Basic to intermediate, calc-alkaline to alkaline, metavolcanic rock, tuff (Witschard 1996) Metaandesite (Bergman et al. 2001)
2. Metasedimentary rock (recrystallised appearance, laminated, locally cross-bedded, more texturally and compositionally uniform than 1, interbedded with 1)	Basaltic andesitic to andesitic (intermediate) volcanogenic epiclastic rock or volcanogenic siltstone to sandstone.	Meta-arenite (Zweifel 1976) Metaarkose (Ros 1980) Meta-arenite (Witschard 1996) Meta-arenite, quartzite (Bergman et al. 2001)
3. Pelite or mica schist (weathers proud, micaceous sheen, may be sericitised, generally intercalated or transitional with 1 and 2, possible textural or compositional variant of 1)	Basaltic andesitic to andesitic (basic to intermediate) fine to very coarse tuff.	Mica schist (Geijer 1918) Pelitic intercalation (Ros 1980) Phyllite to biotite schist (Witschard 1996) Pelite (Martinsson & Wanhainen 2004)
4. Amphibolitic schist (dark greenish grey, foliated, aligned grains, intercalated with 1 and 2, major unit in Linaälven synform hinge area)	Basaltic andesitic (basic to intermediate) fine to very coarse tuff, to fine lapilli-tuff. Locally contains lithic clasts (rare lithic tuff).	Amphibolitic rock (Zweifel 1976) Greenstone intercalation (Ros 1980) Amphibolitic andesite, dacite, trachyandesite (Witschard 1996) Metabasalt (Bergman et al. 2001)
<i>In the Nautanen deformation zone domain (Fig. 2)</i>		
5. Biotite-amphibole schist to gneiss (conspicuous garnet porphyroblasts, pervasively sericitised ± scapolite and K-feldspar-altered, with local biotite-amphibole-magnetite and tourmaline banding. Locally mylonitic. NDZ-hosted equivalent to 1, 3 and possibly 2)	Andesitic to dacitic (intermediate) fine to very coarse tuff, locally agglomeritic tuff (volcanic breccia). Variably sheared, transposed, metasomatised and altered.	High magnetic, biotite-garnet ± amphibole schist to gneiss (Zweifel 1976) Biotite-muscovite-garnet gneiss (Ros 1980) Variably magnetic, basic to intermediate, calc-alkaline to alkaline metavolcanic rock, tuff (Witschard 1996) Metaandesite (Bergman et al. 2001) Shoshonitic metavolcanic rock (McGimpsey 2010)

¹ Protolith volcanoclastic terms based on White & Houghton (2006)

U-Pb SIMS zircon dating of a metavolcaniclastic rock (Nautanen deformation zone)

U-Pb SIMS zircon dating of a feldspar-phyric, intermediate (andesitic) metavolcaniclastic rock from the Nautanen deformation zone was performed to constrain the formational age of the meta-volcanosedimentary sequence. The dated sample (ELH1500085C) was collected from a well-exposed road-cut section that forms part of a variably altered, roughly north-northwest-striking and steeply west-southwest-dipping metavolcaniclastic sequence (cf. Fig. 2).

An outline description of the dated sample and its associated zircon fraction is presented in Table 2. The results of U-Pb SIMS zircon dating are presented in Table 3 (along with an outline of the analytical method). Representative cathodoluminescence (CL) images of the dated zircons and U-Pb concordia and mean ²⁰⁷Pb/²⁰⁶Pb weighted age plots are shown in Figure 10.

In total, ten zircons were analysed, including three crystals with two spots each (i.e. core and rim), giving a total of 13 analyses (Table 3). All of the analyses are concordant or close to concordant, contain

Table 2: Brief description of the metavolcaniclastic rock used for U-Pb SIMS zircon dating

Sample	Setting	Brief sample description	Zircon characteristics
ELH150085C Sweref99 coordinates: E0755910 N7459501	Part of a metavolcaniclastic sequence (<i>Muorjevaara group</i>) within the Nautanen deformation zone (NDZ). The sample area represents a less deformed and altered zone than other parts of the NDZ (consistent with magnetic susceptibility data).	Medium grey, fine- to medium-grained (0.05–3 mm), feldspar-phyric, intermediate (andesitic) metavolcaniclastic rock. Displays weak pervasive sericite \pm K-feldspar \pm magnetite \pm sulphide alteration. Local amphibole-magnetite and quartz veins also occur in the sample area.	Zircons are clear, mostly short (about 30–100 μ m), colourless and rounded (subhedral to anhedral). Cores or overgrowths were not visible under binocular microscope observation. However, CL imaging shows distinct oscillatory zoning in most of the grains, with several containing cores or overgrowths (Fig. 10A).

Table 3. SIMS U-Pb-Th zircon data for the dated meta-andesite sample.

Spot #	U (ppm)	Th (ppm)	Pb (ppm)	Th/U calc* ¹	²³⁸ U/ ²⁰⁶ Pb	$\pm 1\sigma$ (%)	²⁰⁷ Pb/ ²⁰⁶ Pb	$\pm 1\sigma$ (%)	Disc. % conv.* ²	²⁰⁷ Pb/ ²⁰⁶ Pb $\pm 2\sigma$	²⁰⁶ Pb/ ²³⁸ U $\pm 2\sigma$	²⁰⁶ Pb/ ²⁰⁴ Pb measured	$f_{206}\%$ ³		
Sample ELH150085C (meta-andesite, Nautanen area)															
n5397-01a	121.8	75.2	52.9	0.60	2.9595	1.21	0.114052	1.02	0.7	1864.9	36.6	1876.5	39.4	8558	0.22
n5397-01b	93.8	52.6	41.2	0.59	2.9045	1.23	0.112785	1.36	3.9	1844.8	48.8	1907.3	40.8	8781	0.21
n5397-02a	142.2	115.4	65.4	0.81	2.9326	1.19	0.115998	0.88	-0.2	1895.4	31.4	1891.5	39	21997	{0.09}
n5397-02b	120.3	62.4	51.8	0.56	2.9592	1.18	0.113430	1.08	1.3	1855.1	38.8	1876.7	38.6	20507	{0.09}
n5397-03	200.5	158.4	92.0	0.80	2.9324	1.08	0.115623	0.73	0.1	1889.6	26.0	1891.5	35.4	46695	{0.04}
n5397-04	91.5	65.6	40.1	0.68	3.0037	1.28	0.115496	1.08	-2.1	1887.6	38.6	1852.6	41.2	15722	{0.12}
n5397-05	191.9	156.5	88.3	0.83	2.9337	1.09	0.113559	0.78	2.1	1857.1	28.0	1890.8	35.8	12960	0.14
n5397-06	70.7	39.2	30.5	0.55	2.9653	1.29	0.116561	1.21	-1.9	1904.1	43.4	1873.3	42.2	15010	{0.12}
n5397-07	104.4	66.7	42.2	0.61	3.1822	1.19	0.108535	1.21	-0.9	1775.0	44.0	1761.6	36.8	5463	0.34
n5397-08	250.2	260.7	121.1	1.06	2.9089	1.05	0.113059	0.68	3.5	1849.2	24.4	1904.8	34.6	13601	0.14
n5397-09	131.0	87.9	58.2	0.69	2.9478	1.19	0.113900	0.93	1.3	1862.5	33.4	1883.0	38.8	13604	0.14
n5397-10a	159.2	129.1	73.7	0.83	2.9148	1.10	0.114464	0.86	1.9	1871.5	30.8	1901.5	36.4	11157	0.17
n5397-10b	129.2	103.7	58.9	0.80	2.9434	1.18	0.114416	1.10	0.9	1870.7	39.2	1885.4	38.6	15564	0.12

Isotope values are common Pb-corrected using modern common Pb composition (Stacey & Kramers 1975) and measured ²⁰⁴Pb. Data row with strikethrough text was not used in the concordia or mean weighted age determinations

*¹ Th/U ratios calculated from ²⁰⁸Pb/²⁰⁶Pb and ²⁰⁷Pb/²⁰⁶Pb ratios, assuming a single stage of closed U-Th-Pb evolution

*² Age discordance in conventional concordia space. Positive numbers are reverse discordant.

*³ Common Pb fraction. Figures in parentheses are given when no correction has been made, and indicate a value calculated assuming present-day Stacey-Kramers common Pb.

relatively low concentrations of U (approximately 71–250 ppm), and have Th/U ratios of 0.55–1.06. The spread in ²⁰⁷Pb/²⁰⁶Pb apparent ages for the 13 analyses (c. 1.90 to 1.78 Ga) and their corresponding standard deviations (2 σ) are relatively large, probably due to low total Pb concentrations (approximately 31–121 ppm, Table 3). One concordant analysis (spot n5394-07, Fig. 10A, Table 3) has a distinctly younger ²⁰⁷Pb/²⁰⁶Pb apparent age of 1775 ± 44 Ma (2 σ) and was not included in the final age determination. The remaining 12 analyses have ²⁰⁷Pb/²⁰⁶Pb ages that overlap at the 2 σ -level (Fig. 10C).

U-Pb SIMS dating method: Zircons were obtained from a density separate of a crushed rock sample using a Wilfley water table. Magnetic minerals were removed using a hand magnet. Handpicked zircons

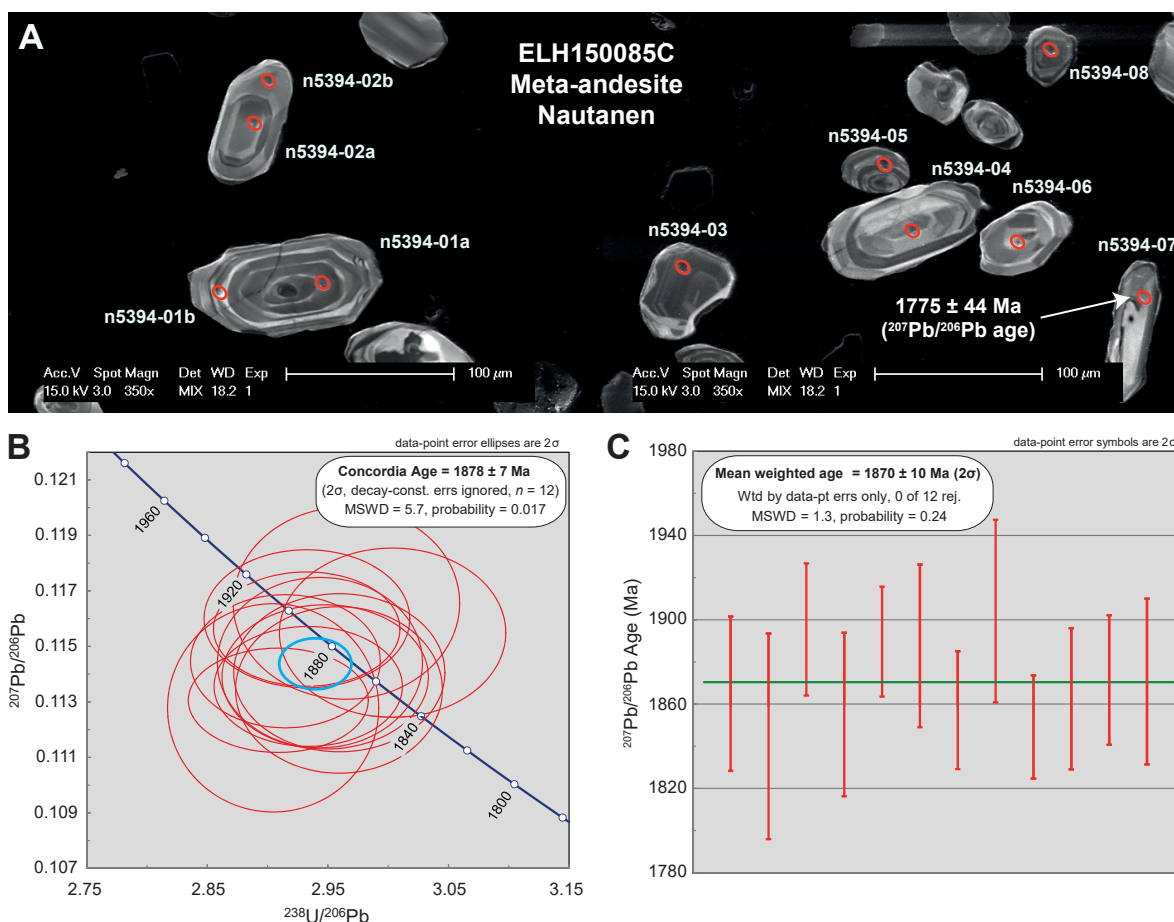


Figure 10. U-Pb SIMS zircon geochronology results for metavolcaniclastic rock sample ELH150085C (meta-andesite) from the Nautanen area (see Fig. 2). **A.** Cathodoluminescence images of representative zircons obtained from the sample. Red ovals and corresponding labels represent analytical dating spots. The zircon containing analytical spot n5394-07 yielded a significantly younger concordant $^{207}\text{Pb}/^{206}\text{Pb}$ age of 1775 ± 44 Ma (2σ), and was excluded from the final calculated age (Table 3). **B.** Tera-Wasserburg plot for the zircon population ($n = 12$). The blue oval represents the calculated concordia age of 1878 ± 7 Ma (2σ). **C.** Mean weighted $^{207}\text{Pb}/^{206}\text{Pb}$ age plot for the zircon population.

were mounted in transparent epoxy resin together with chips of reference zircon 91500. The zircon mounts were polished, gold coated and examined by cathodoluminescence imaging at the Swedish Museum of Natural History (NRM), Stockholm. High-spatial resolution secondary ion mass spectrometer (SIMS) analysis was carried out using a Cameca IMS 1280 at the NordSIM facility at the NRM. Detailed descriptions of the analytical procedures are given in Whitehouse et al. (1997, 1999), and Whitehouse & Kamber (2005). An approximately 6 nA O^{2-} primary ion beam was used, yielding spot sizes of approximately 15 μm . U/Pb ratios, elemental concentrations and Th/U ratios were calibrated relative to the zircon 91500 reference, which has an age of c. 1065 Ma (Wiedenbeck et al. 1995, 2004). Common Pb-corrected isotope values were calculated using modern common Pb composition (Stacey & Kramers 1975) and measured ^{204}Pb values in cases where the ^{204}Pb count rate was above the detection limit. U and Th decay constants follow the recommendations of Steiger & Jäger (1977). Diagrams and age calculations of isotopic data were made using Isoplot 4.15 software (Ludwig 2012). All age uncertainties are presented at the 2σ or 95% confidence level.

On a Tera-Wasserburg plot (Fig. 10B), 12 analyses plot as an overlapping concordant to near-concordant group, and yield a concordia age of 1878 ± 7 Ma (2σ , $n = 12$, MSWD = 5.7, probability of concordance = 0.017). A degree of reverse discordance, where several points plot to the left of the con-

cordia line, may account for the relatively high MSWD value. The corresponding mean weighted $^{207}\text{Pb}/^{206}\text{Pb}$ age of these 12 points is 1870 ± 10 Ma (2σ , MSWD = 1.3, probability = 0.24; Fig. 10C). The U-Pb concordia age and the mean weighted age overlap at the 2σ -level and the former is chosen as the best estimate for the crystallisation age of the metavolcaniclastic sample (i.e. c. 1.88 Ga).

Several zircons display textural characteristics suggesting core-mantle overgrowth relationships, and have corresponding $^{207}\text{Pb}/^{206}\text{Pb}$ ages, indicating possible age heterogeneity (Fig. 10A, Table 3). For example, the core domain of zircon 2 (spot 02a) has a $^{207}\text{Pb}/^{206}\text{Pb}$ age of 1895 ± 31 Ma (2σ), whereas the mantle domain (spot 02b) has an age of 1855 ± 39 Ma (2σ). While both ages overlap at the 2σ -level, it is possible that the core is inherited (i.e. represents c. 1.90 Ga inherited material). The presence of older inherited material is further evidenced by a single analysis of the core domain of crystal 6 (spot 06), which yielded a $^{207}\text{Pb}/^{206}\text{Pb}$ age of 1904 ± 43 Ma (2σ). For zircon 1 (Fig. 10A), which displays both oscillatory and core-overgrowth characteristics (e.g. curved zone boundaries in the latter case), the age difference between the inner and outer domains is smaller, with spot 01a (closer to the core) yielding a $^{207}\text{Pb}/^{206}\text{Pb}$ age of 1865 ± 36 Ma (2σ), and spot 01b (outer mantle domain) giving 1845 ± 48 Ma (1σ). While these ages again overlap at the 2σ -level, a real age difference between the central and peripheral parts of the crystal is possible, similar to that obtained for zircon 2.

The new U-Pb SIMS zircon age of 1878 ± 7 Ma for the metavolcaniclastic unit from the Nautanen deformation zone constrains the timing of the Svecofennian intermediate (andesitic) volcanism that deposited the Muorjevaara group sequence and represents the first robust formational age for volcanoclastic- and epiclastic-type deposits in the broader Nautanen–Gällivare area. Additionally, given the general petrographic and lithogeochemical similarities across the meta-volcanosedimentary sequence from the Aitik area in the south to the northern part of the study area (see *Lithogeochemistry section* above; cf. Monro 1988), the new U-Pb date provides the most precise constraint on the age of metavolcaniclastic wall rocks hosting the Nautanen IOCG and Aitik Cu-Au-Ag deposits.

The U-Pb age of 1878 ± 7 Ma for the Nautanen meta-andesite overlaps other ages determined for a variety of rock units in the Nautanen–Aitik and adjacent areas. The new date is identical to a U-Pb LA-ICP-MS zircon “minimum age” of 1878 ± 7 Ma for a meta-andesite located approximately 100 km northwest of Gällivare, hosting the Fe-Cu ± Au system at Tjärrojåkka (Edfelt et al. 2006). The Nautanen meta-andesite age also overlaps new U-Pb SIMS zircon dates of 1883 ± 4 Ma for the mafic-ultramafic Dundret complex (southwest of the study area), and 1870 ± 4 Ma for a dioritic intrusion west of the Nautanen deposit (Fig. 2; Sarlus 2016). Moreover, the c. 1.88 Ga age overlaps c. 1.89–1.88 Ga igneous ages reported for dioritoid and granitoid intrusions in the Aitik area (Wanhainen et al. 2006, Sarlus 2016) and suggests that the dioritic bodies are the intrusive equivalent of the mainly intermediate meta-volcanosedimentary sequence (cf. Witschard 1996, Wanhainen et al. 2012). Additionally, the oldest sulphide mineralisation at Aitik, constrained at c. 1.88 Ga by Re-Os molybdenite dating, and inferred to relate to an initial “porphyry Cu” mineralisation event (Wanhainen et al. 2005, 2006), coincides with the c. 1.88 Ga phase of intermediate magmatism dated in this study.

Overall, the geochronology results reported here, combined with additional petrographic, geochemical and geochronological data, confirm a temporal and probable genetic link between Muorjevaara group metasupracrustal rocks and compositionally similar dioritic to granitic intrusions in the area, and highlight an important phase of syn-orogenic, mafic to intermediate magmatism at c. 1.88 Ga. Additionally, several zircon cores record $^{207}\text{Pb}/^{206}\text{Pb}$ ages from c. 1.90 to 1.89 Ga, suggesting inheritance of marginally older volcanic ± plutonic material not exposed at the present erosion level. These data partly affirm tentative U-Pb LA-ICP-MS ages of c. 1.90 Ga for the core domains of titanite crystals obtained from altered metavolcanic rocks hosting the Malmberget iron mine (Storey et al. 2007), which suggest those rocks are older than the Nautanen package investigated in this study (cf. Fig. 3). Combined, the older temporal signatures imply that a substrate of c. 1.90 to 1.89 Ga rocks may have been recycled during the c. 1.88 Ga tectonothermal event.

Intrusive rocks and their relationship to the Muorjevaara group

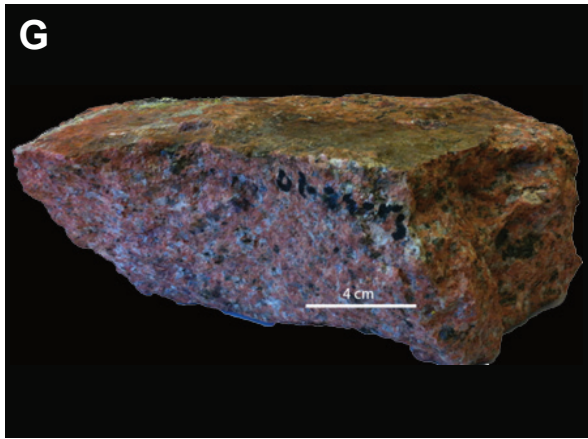
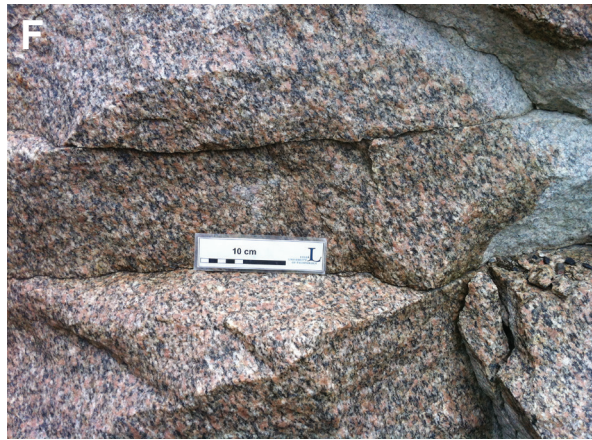
To the north, east and west of the Nautanen area, the Muorjevaara group is intruded by relatively abundant plutonic and hypabyssal rocks (Fig. 2). These consist of (1) generally foliated and locally folded, medium to coarse-grained, c. 1.88 to 1.87 Ga dioritic to granodioritic plutons (Fig. 11A & E–F); (2) c. 1.81 to 1.80 Ga gabbroic to doleritic and syenitic intrusions (Fig. 11H); and (3) voluminous, weakly deformed to massive, c. 1.79 to 1.78 Ga granitic intrusions (Fig. 11C & G, e.g. Witschard 1996, Sarlus 2016). The older c. 1.88 Ga dioritic intrusions were emplaced at approximately the same time as the c. 1.88 Ga mafic-ultramafic Dundret complex to the southwest (cf. Sarlus 2016). Thus, two broad episodes of bimodal plutonism at c. 1.88 Ga and c. 1.80 Ga are recognised in the general Gällivare area (see also Sarlus et al. 2017).

Locally exposed intrusive contacts in the Nautanen area provide rare field evidence of the temporal relationship between intrusive rocks and Muorjevaara group units, and help establish the number and sequence of intrusive events (Fig. 11). Dioritic and granitic bodies of varying size intrude the sequence, typically parallel to primary bedding and dominant foliations (i.e. sills), or as discordant veins or dykes with moderate to high angles relative to planar fabrics (Figs. 11B–D).

In the Eastern volcanosedimentary domain, fine- to medium-grained (approximately 0.5–3 mm), dioritic dykes and veins intrude metavolcaniclastic rocks with sharp contacts (Fig. 11B). These minor intrusions resemble larger-scale, medium- to coarse-grained (approximately 1–8 mm), diorite to quartz monzodiorite bodies in the area (e.g. c. 1.89 Ga Aitik stock), and contain similar textural and lithological features (e.g. mafic enclaves, Fig. 11A).

Granitic rocks also crosscut the meta-volcanosedimentary sequence with sharp, igneous contacts and typically intrude parallel to primary and overprinting structures (Fig. 11C–D). They occur as fairly abundant, approximately 1–15 m thick, medium- to coarse-grained (approximately 1–10 mm), granitic to locally pegmatitic, sills and minor, approximately 1–5-cm-thick, fine- to medium-grained (approximately 0.5–5 mm) aplite veins and segregations (Fig. 11C–D). Where present, granitic veins consistently crosscut dioritic bodies (Fig. 11A), and thus reflect the absolute ages of these intrusive suites in the general Gällivare area (cf. Sarlus 2016).

► Figure 11. Intrusive rocks and field relationships. **A.** View to the southwest of weak to moderately foliated monzodiorite (Haparanda suite) with mafic microgranular enclave (arrow). Crosscutting northwest-aligned aplite vein is seen near the top. **B.** Bedding view (to the northeast) of well-sorted, laminated, intermediate metavolcaniclastic rock cut by west-northwest-aligned, dioritic veins. Note elongate mafic enclaves in the veins (arrows), which are compositionally similar to the enclave shown in A. **C.** View to the north-northeast of contact (broken line) between reddish-pink, massive granite sill and biotite schist. **D.** Bedding view (to the southwest) of northwest-aligned, laminae-parallel, aplite veins crosscutting magnetite-bearing biotite schist. **E.** Intermediate, medium-grained dioritic rock predominantly comprising amphibole and plagioclase (Haparanda suite). **F.** Example of a moderately deformed (foliated), pale pink Lina-type granite. **G.** Undeformed, coarse-grained, Lina-type granite with distinct pinkish colour. **H.** Reddish-pink, K-feldspar-rich syenitic intrusion (possibly Perthite monzonite suite). Photographs A–D by Edward Lynch. Photographs E–H by Zmar Sarlus.



STRUCTURAL GEOLOGY AND DEFORMATION

Structures in the eastern volcanosedimentary domain

The eastern volcanosedimentary domain (EVD) contains a variety of superimposed ductile and brittle structures recording a protracted, multiphase deformation history. The most commonly observed fabric is a variably intense, planar penetrative foliation, here designated S1 (Figs. 12A–B). This foliation is generally roughly northwest to north-northwest-aligned, moderate to steeply southwest to west-southwest-dipping, and tends to parallel primary bedding, laminae and compositional banding. S1 has a similar orientation to planar foliations in EVD-hosted dioritic intrusions. The intensity of S1 varies between outcrop and lithology, and where it forms a schistose to gneissic texture, S1 may represent a composite transposed foliation (cf. Fig. 5). Locally, S1 is axial planar to tight to isoclinal, asymmetric, intrafolial F1 folds (Fig. 12B).

The EVD is also characterised by tight to isoclinal folding of primary bedding, compositional banding, alteration banding and foliations. To the immediate east of the Nautanen deformation zone (i.e. southern EVD) the predominant structure is a distinct, large-scale, asymmetrical and overturned syncline (cf. Fig. 2). The western limb appears to be truncated roughly north-northwest-trending, shear zones and faults related to the Nautanen deformation zone. Fold vergence is typically eastward, with axial surfaces roughly north to north-northwest-aligned (sub-parallel to the Nautanen deformation zone) and generally dips steeply towards the west. The fold shapes are non-cylindrical and fold axes are locally curvilinear. The larger-scale fold structures are accompanied by parasitic, asymmetric small-scale folding. In the southern part of the EVD, parasitic fold axes commonly plunge at moderate angles towards the south-southwest, whereas in the north fold axes have doubly plunging geometries (typically roughly northwest and southeast). Mineral lineations are gently plunging and have varying orientations.

A discordant c. bedding plane-orthogonal crenulation cleavage, here designated S2, also occurs in the EVD (Fig. 10C–D). It is generally roughly north to north-northeast-aligned, sub-vertical and is axial planar to gentle, upright, moderate roughly south to south-southeast-plunging F2 folds (Fig. 10C). The S2 cleavage is associated with L2 intersection lineations that typically have a moderate plunge to the south and south-southeast, similar to F2 fold axes. Locally, near the hinge zones of larger-scale folds, fairly intense S2–L2 deformation has developed elongate and stretched L-tectonites, which form mullion-like features along bedding surfaces (Fig. 10E). In eastern limb areas local bedding plane surfaces with L2 lineations contain slicken-side notches, indicating top-block reverse movement towards the north and north-northwest (Fig. 10F).

Brittle deformation in the EVD consists of (1) locally developed spaced cleavage and fracture sets that tend to follow earlier planar structures; (2) numerous roughly north-northwest- and east-aligned, generally sub-vertical, amphibole and quartz vein sets, of which the latter are locally sulphide-bearing (e.g. Ferrum Cu-Au prospect); and (3) joint sets developed in intrusive rocks. Additionally, discordant roughly north to north-northeast-aligned brittle deformation zones are inferred from aeromagnetic data (cf. Fig. 2). These crosscutting, locally NDZ-related high-strain zones segment the EVD into several localised blocks (see below).

Structures in the Nautanen Deformation Zone

The Nautanen deformation zone (NDZ) is an important regional-scale, composite shear zone in northern Norrbotten and is the most prominent large-scale structural feature in the study area (e.g. Bergman et al. 2001). Here, it occurs as a somewhat dilational, approximately 300 m to 2 km wide high-strain deformation zone, characteristically delineated on aeromagnetic maps by planar, sub-parallel, roughly north-northwest-aligned magnetic anomalies (cf. Fig. 14).

Structurally, the NDZ is characterised by a conspicuous roughly north-northwest to northwest-

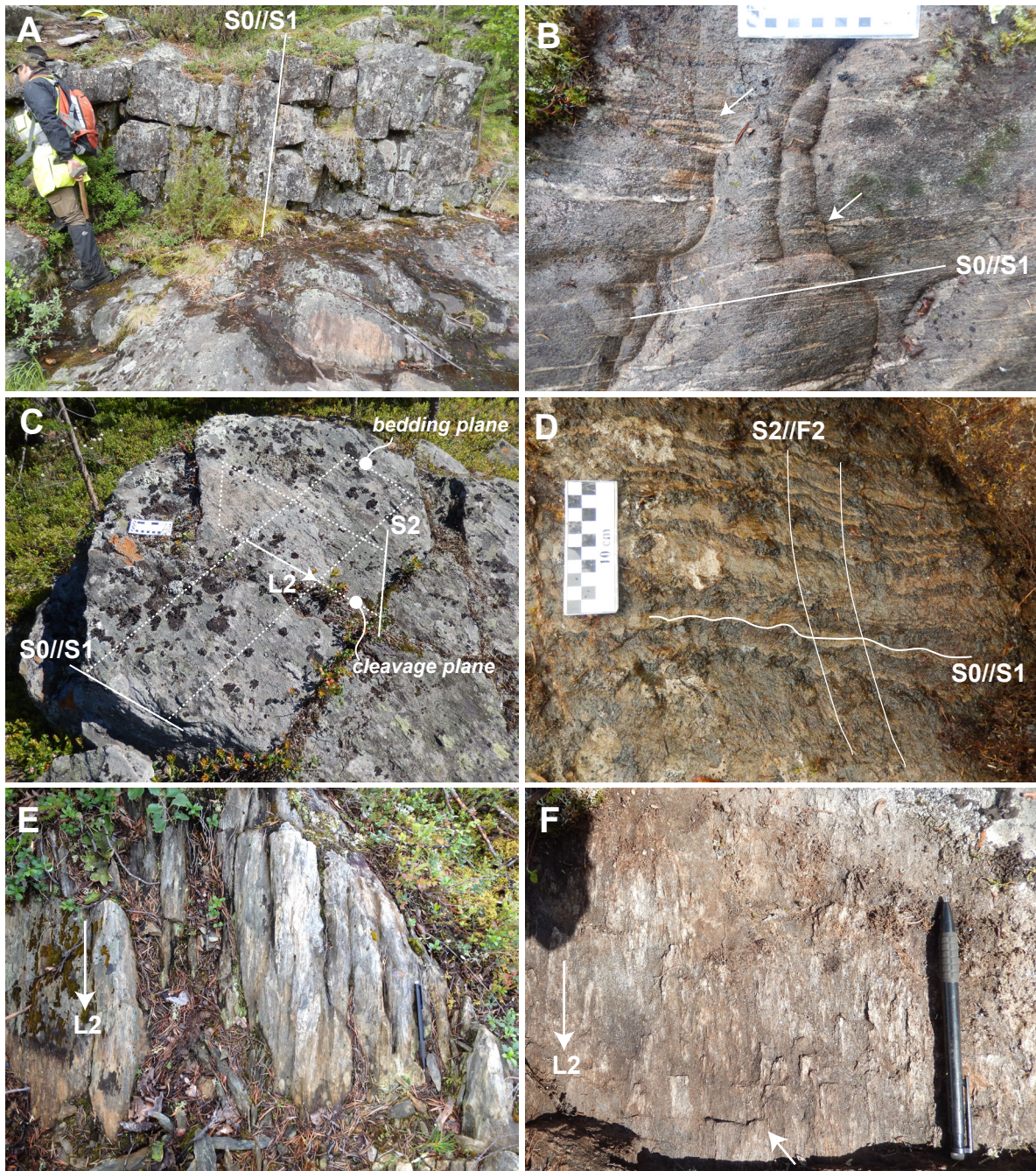


Figure 12. Examples of structures in the eastern volcanosedimentary domain. **A.** North-northeast view of steeply west-south-west-dipping, medium-bedded metavolcaniclastic rocks with bedding-parallel S_1 foliation. Zmar Sarlus for scale. **B.** Side surface view (to the east-northeast) of laminated and compositionally banded mica schist with dominant bedding-parallel S_1 foliation. Arrows indicate tight to isoclinal, recumbent, interfolial folding (F_1) of feldspathic bands and veins. **C.** View to the northeast of mica schist showing bedding-cleavage relationship and related south-southeast-plunging L_2 intersection lineations. **D.** Top surface view (to north-northeast) of compositionally banded metasedimentary rock, showing bedding-parallel S_1 foliation affected by steep S_2 cleavage, axial planar to gentle, upright, south-southeast-plunging F_2 folds. **E.** Top surface view (to the north-northwest) of mica schist with stretched south-southeast-plunging L_2 intersection lineation associated with mullion-like features. **F.** Bedding surface view (to the north) showing moderate, south to south-southeast-plunging L_2 intersection lineations. Arrow marks slicken-side notches, which suggest top block movement towards the north. All photographs by Edward Lynch.

aligned, steep to locally moderate roughly west-dipping, penetrative foliation (S1), with varying but generally strong intensity (Fig. 13A–B). Locally, inferred primary bedding, compositional banding and alteration banding are typically transposed into steep orientations parallel to the dominant foliation, and locally produce a composite fabric that may represent several generations of ductile deformation. The dominant shearing direction strikes roughly north-northwest and shows mainly western-block up reverse kinematics and most commonly oblique dextral and less common sinistral components, recorded by asymmetric foliation deflections around garnet porphyroblasts and local asymmetric kink bands (Fig. 13C–E).

The predominant north-northwest-trending reverse shear zones within the NDZ are interconnected by roughly north-trending, sub-vertical high-strain zones with mainly dextral kinematics. In general, these secondary zones are interpreted as Riedel shears that formed in the oblique, dextral-reverse shear zone (Fig. 14). Additionally, local tensional features such as quartz-filled tension gashes and en-echelon quartz veins occur along the western margin of the NDZ, and are mainly orientated north to north-northeast.

Minor asymmetric folding related to shearing is mainly evident from asymmetrically folded hornblende-, magnetite- and epidote-filled veinlets (Fig. 13F). To the south of the study area, at the Aitik deposit (Fig. 14), the reverse shear zones are more N–S orientated and dip moderately towards the west, with distinct roughly west-plunging mineral lineations. Additionally, a set of sub-vertical, north-northeast-trending high-strain zones is observable. It has been suggested that it controls the distribution of gold in the Aitik deposit (Sammelin 2011).

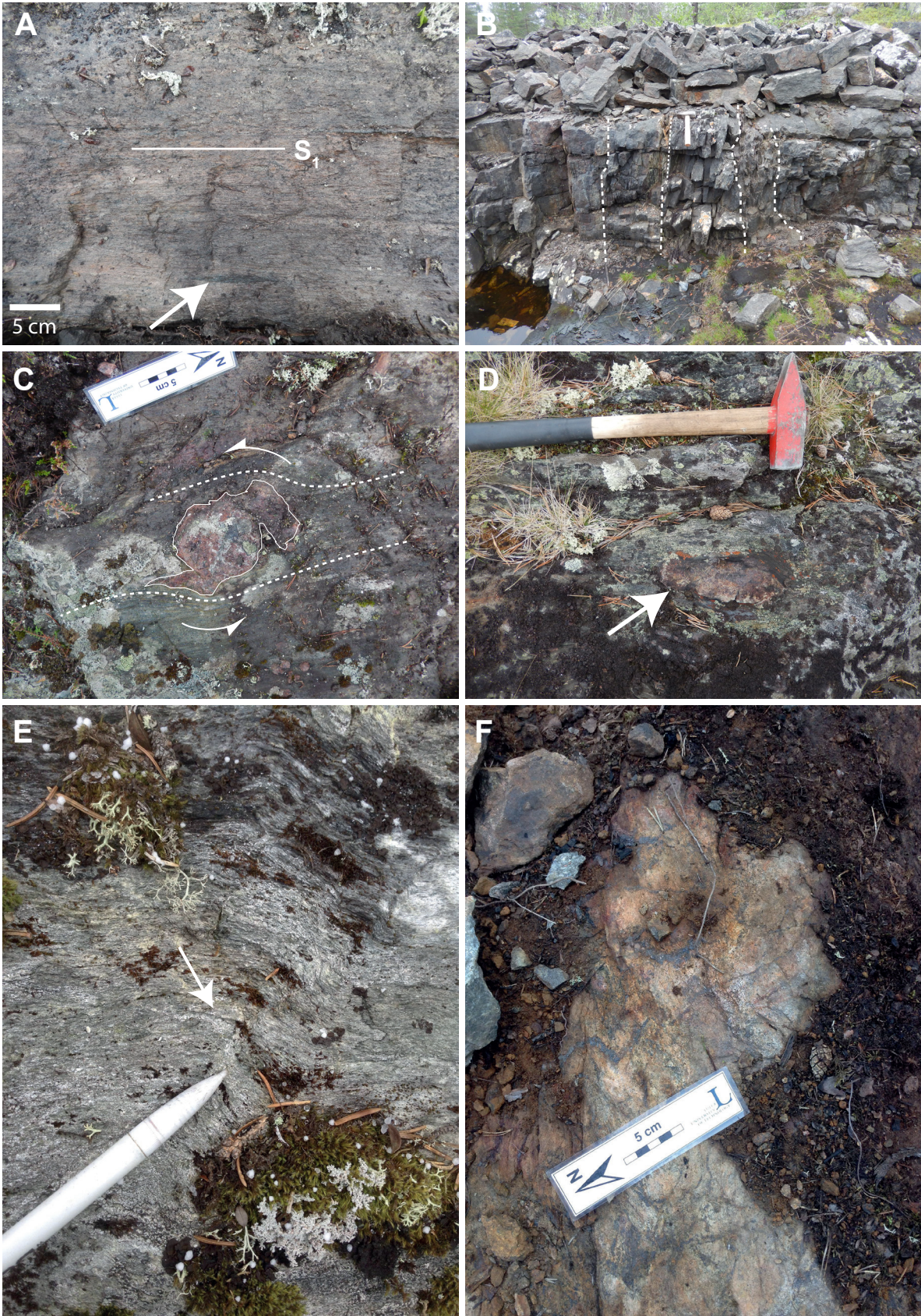
Mineral lineations in the NDZ are defined by stretching of minerals, and their orientations are variable. In general, lineations plunge moderately towards the south and southwest. Local variations, with gentle to horizontal plunges, were also observed.

Structures in the western volcanosedimentary domain

The western volcanosedimentary domain (WVD) is characterised by alternating layers of metasedimentary and meta-volcanosedimentary rocks, with a distinct bedding (S0) and parallel foliation (S1) forming a composite S0-1 fabric. Both bedding and the S1 foliation are folded into inclined to overturned asymmetric folds, with open to close interlimb angles. The predominant large-scale structure in the WVD is a repetition of anticlines and synclines, with non-cylindrical, curvilinear fold axis (see Fig. 2). The overall orientation of fold axes is southward with gentle to moderate plunges. Fold axes in the northwest of the WVD appear to be doubly-plunging.

Typically, an axial planar parallel fabric is not observed across the WVD. Nevertheless, a weak foliation or weak-spaced cleavage, here designated S2, could be observed in several outcrops, especially in the vicinity of the NDZ. This S2 fabric clearly overprints the S0-1 foliation obliquely (Fig. 15A).

► Figure 13. Examples of structures in the Nautanen deformation zone domain. **A.** Top surface view (to the west-south-west) of dominant, steeply west-southwest-dipping, penetrative S1 schistosity affecting biotite-magnetite-altered metavolcaniclastic rocks. Arrow indicates altered and stretched clast replaced by biotite. **B.** Along-strike side view (to the south-southeast) showing localised high-strain shearing (broken lines) of altered schist. **C.** Top surface view (to the west) of garnet porphyroblast partly deflecting S1 fabrics in schist. Deflection pattern and garnet growth tails indicate possible dextral rotation. **D.** Top surface view (to the west-southwest) of elongate (stretched?) garnet porphyroblast (arrow) in biotite-magnetite-altered schist. **E.** View to the southwest of small-scale dextral kink bands (arrow) in mica schist. **F.** View to the south-southeast (along strike) of asymmetric folding of magnetite-filled veinlets in mica-amphibole schist. All photographs by Edward Lynch, except E and F by Tobias Bauer.



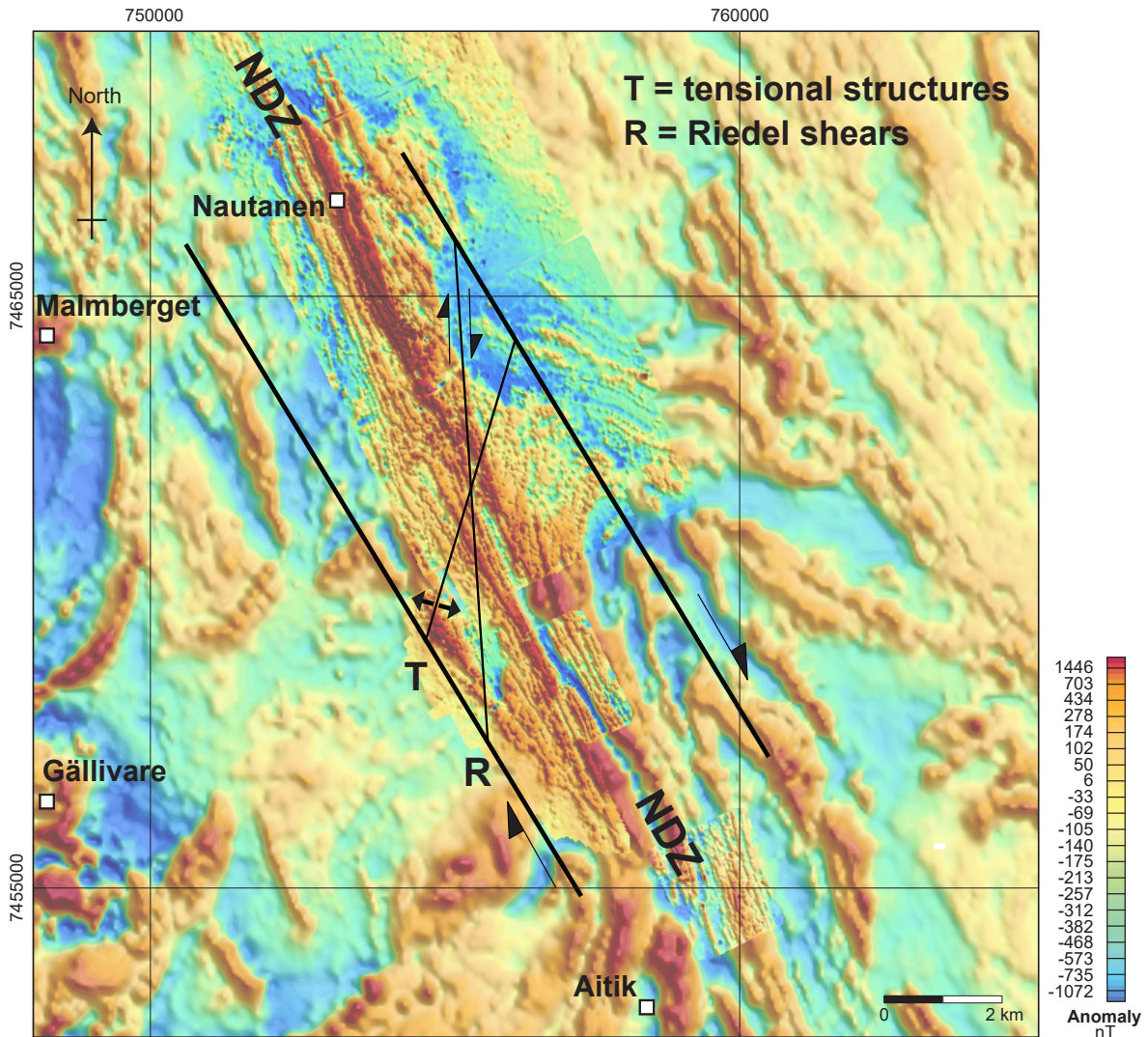


Figure 14. Conceptual model of primary, secondary and tertiary structures along the Nautanen deformation zone (NDZ). The background image is merged data from airborne and ground magnetic measurements.

Local crenulation lineations, small-scale fold axes and mineral-stretching lineations are orientated sub-parallel to the larger-scale fold axes (Fig. 15B–D).

Brittle deformation in the WVD is dominated by a large-scale, northwest-striking fault zone that divides the foliated and folded metavolcanic and metasedimentary rocks to the north from mainly undeformed granites to the south (Fig. 2). The fault zone is characterised by intense fracturing forming distinct topographic depressions.

Structures associated with intrusive rocks

Intrusive rocks in the area have varying strain intensities that reflect their relative ages and emplacement histories. A general penetrative foliation is seen in Haparanda-type dioritic to granodioritic intrusions (Fig. 16A). In the eastern domain, it is predominantly north-northwest to northwest-aligned, steeply southwest-dipping, and tends to follow the orientation of the predominant S1 foliations seen in the country rocks. Locally, dioritic dykes intruding metavolcanic rocks display evidence of dextral-oblique emplacement associated with folding (e.g. Fig. 16B), while high-strain zones cutting

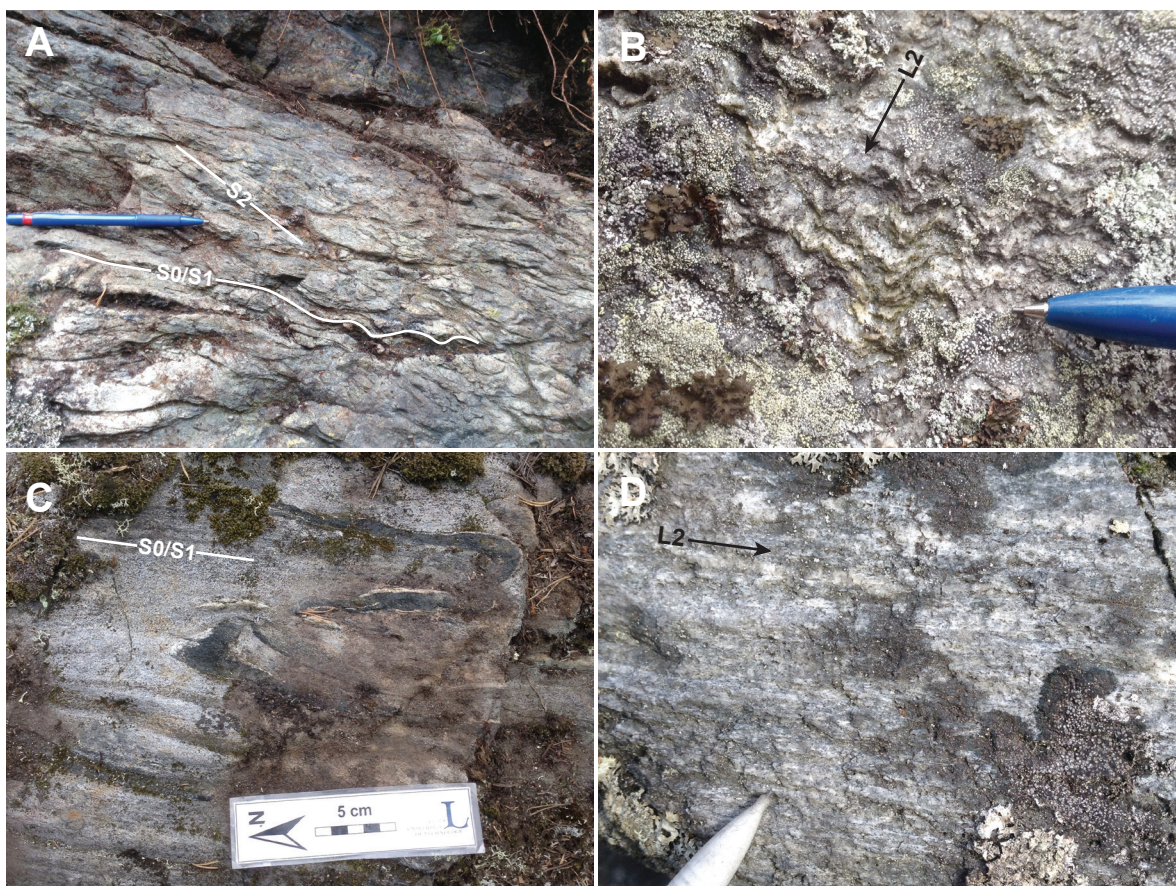


Figure 15. Examples of structures in the western volcanosedimentary domain. **A.** Mica schist, showing schistosity-cleavage relationship (S_0 -1 and S_2 , respectively). View to the east. **B.** Small-scale folds, with L_2 crenulation lineations parallel to axial planes. View to the east-northeast. **C.** View to the east of metavolcaniclastic rock and folded vein. **D.** View to the east of L_2 intersection lineation in an intermediate metavolcaniclastic rock. All photographs by Tobias Bauer.

through the dioritic intrusions can cause a strong transposition of the penetrative foliation, suggesting local pre-shearing emplacement. Along the western margin of the Nautanen deformation zone, dioritic intrusions occur as narrow, elongate, north-northwest-aligned bodies that are orientated sub-parallel to, and deflected by, folding and Nautanen deformation zone-related shearing (cf. Fig. 2). Overall, the foliated character of the dioritic rocks, combined with their general orientation and intrusive patterns, suggests a probable syn-kinematic emplacement (cf. Witschard 1996).

Lina-type granitic rocks and subordinate aplite-pegmatite bodies typically occur as sheet-like intrusions, sills and veins intruding parallel to planar structures (cf. Fig. 11). A varying degree of strain is observable in these granitic rocks, ranging from penetratively foliated to non-foliated (cf. Fig. 11F–G). This suggests episodic emplacement of several generations of granitic rocks in the area and indicates that not all granitic intrusions may strictly belong to the Lina suite association (cf. Bergman et al. 2001).

Variably deformed granitic rocks are also known from the broader Gällivare area. For example, Wanhainen et al. (2005) report radiometric ages for both deformed and undeformed pegmatitic dykes occurring at the Aitik deposit, south of Nautanen. A deformed pegmatite dyke yielded an age of c. 1.85 Ga, while undeformed dykes have ages from c. 1.76 to 1.73 Ga. In addition, Bergman et al. (2002) obtained an age of c. 1.77 Ga from a weakly foliated, Lina granite roughly 30 km NW of the Nautanen area. These data, combined with observations presented here, support the contention that both syn- and post kinematic granite magmatism occurred in the general Gällivare area.

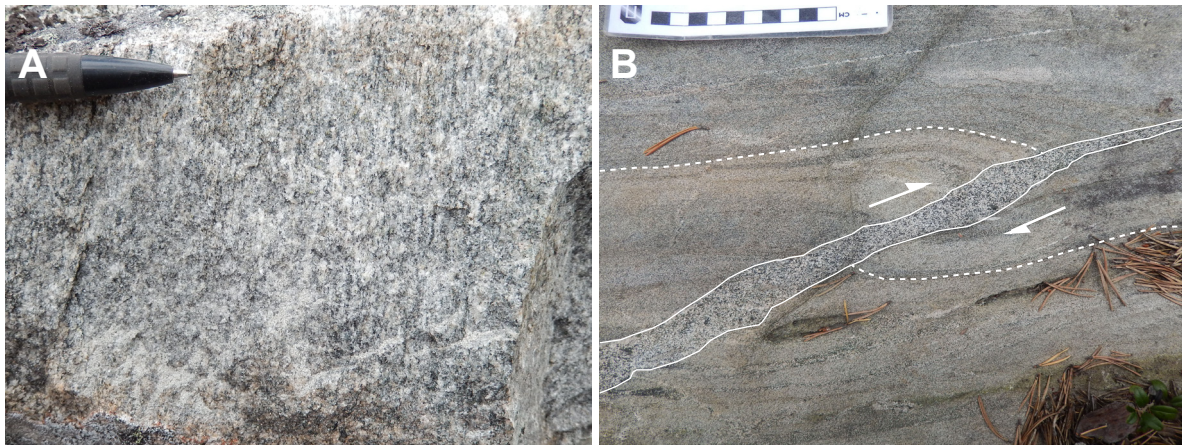


Figure 16. **A.** Sub-vertical surface view to the north-northwest of sub-vertical foliation in medium-grained, monzodioritic intrusion. **B.** Sub-horizontal surface view to the southwest of dioritic dyke crosscutting steeply south-southwest-dipping, thinly laminated, metavolcaniclastic rock. Laminae appear dextrally offset and associated with possible syn-emplacment drag fold (broken lines). All photographs by Edward Lynch.

Geophysical modelling of the Nautanen Deformation Zone

The study area was investigated in five separate airborne geophysical campaigns between the early 1960s and the mid-1990s, which resulted in the acquisition of magnetic, radiometric and electromagnetic data (slingram and VLF). Additionally, regional-scale ground gravity measurements have been conducted using approximately 1.5 km station spacing. Petrophysical sampling, ground magnetic and ground slingram measurements have also been made (cf. Lynch & Jönberger 2014).

From a magnetic anomaly perspective, the western volcanosedimentary domain (WVD) is relatively heterogeneous, with a banded pattern (Fig. 17). The low-magnetic parts of the area mainly consist of metasedimentary or felsic metavolcaniclastic rocks, while the high-magnetic bands are caused by mafic to intermediate metavolcaniclastic rocks. Mafic intrusive rocks also have relatively high magnetisation values (Table 4). On the gravity map a regional trend dipping towards the west indicates that granitic intrusions in this area have a deeper depth extent (Fig. 18).

The NDZ domain has been the target of both ground magnetic and ground slingram surveys in the past (cf. Lynch & Jönberger 2014). The magnetic anomaly map shows historical ground magnetic measurements overlaying airborne magnetic data, and displays a zone of tight, sub-parallel magnetic bands corresponding to the NDZ (Fig. 17). On the gravity map, the NDZ correlates with a broad positive gravity anomaly, implying that more mafic lithologies (higher density) underlie the NDZ than in surrounding areas (Fig. 18). The positive gravity anomaly extends eastwards from the central NDZ towards gabbroic rocks at Snålkok (cf. Fig. 2).

The eastern volcanosedimentary domain (EVD) mainly consists of intercalated metavolcanoclastic or metasedimentary rocks. Intrusive rocks in the area range from granite to gabbro. On the magnetic anomaly map the area resembles the pattern for the WVD, with high-magnetic bands alternating with areas with lower magnetic signatures. A synformal fold in the southern part of the EVD can also be observed on the magnetic anomaly map. The high-magnetic bands consist of mafic metavolcaniclastic rocks, whereas the lower magnetic areas are metasedimentary rocks. In the north of the EVD a granitic intrusion correlates well with a low gravity anomaly. Further south, the sequence of alternating metasedimentary and metavolcaniclastic rocks have roughly the same densities and give rise to a positive anomaly on the gravity map (Table 4). In the central and eastern part of the EVD, a homogeneous low-magnetic area on the magnetic anomaly map corresponds to mafic intrusive rocks. Low-magnetic granite is seen as a gravity low in the far southeast of the EVD.

Three 3D models have been constructed of the NDZ by the inversion of gridded ground magnetic

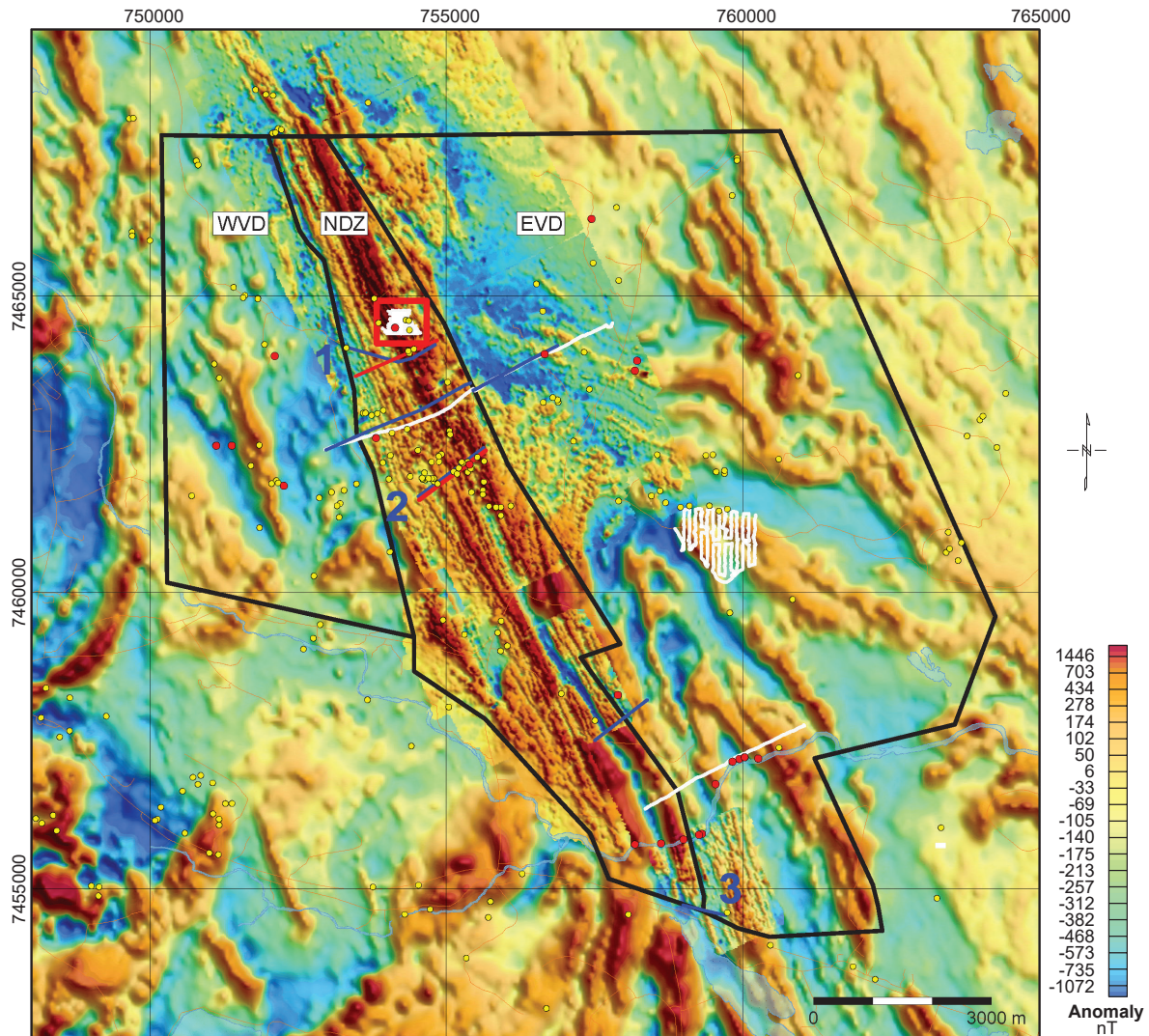


Figure 17. Magnetic anomaly map of the Nautanen area. Airborne data is overlain by ground magnetic data, acquired in previous surveys. The black polygons represent study area domains. The white and blue lines correspond to new ground magnetic and VLF measurements, respectively (this study). Petrophysical samples acquired earlier are shown as yellow dots, newer samples with red dots. The numbers “1–3” correspond to profiles discussed in the main text, and relate to Figs. 21–24. The red box surrounding the Nautanen Cu-Au deposit is presented in Figure 19. The red lines show the extent of extracted cross-sections from 3D VOXI models, shown in Figures 21 and 23.

data in the VOXI environment developed by Geosoft (Figs 20, 21 & 23). The aim of this modelling was to visualise highly magnetised structures in the sub-surface and their geometrical behaviour at shallow depth (down to approximately 200 m).

The most northerly 3D inversion model was made of the Nautanen Cu-Au deposit and surrounding area (red rectangle in Figs. 17 & 18). The input data to the model was newly acquired ground magnetic data along parallel profiles striking east-west that were collected with an individual spacing of 10 m (Fig. 19). Measurements of the magnetic field were recorded along these profiles approximately once a metre. The 3D model was confined to 300 m in an east-west direction and 400 m in a north-south direction (Fig. 19). The cell size of each volume pixel (voxel) in the model is 5 × 5 m horizontally, and a few metres vertically.

Before the data were inverted, the voxels were assigned minimum and maximum constraints for their permitted magnetic susceptibilities. Due to the occurrence of very high-magnetic bands in the area, constraints on susceptibility were set between 0 and 2 SI units. One cross-section (Fig. 20) has

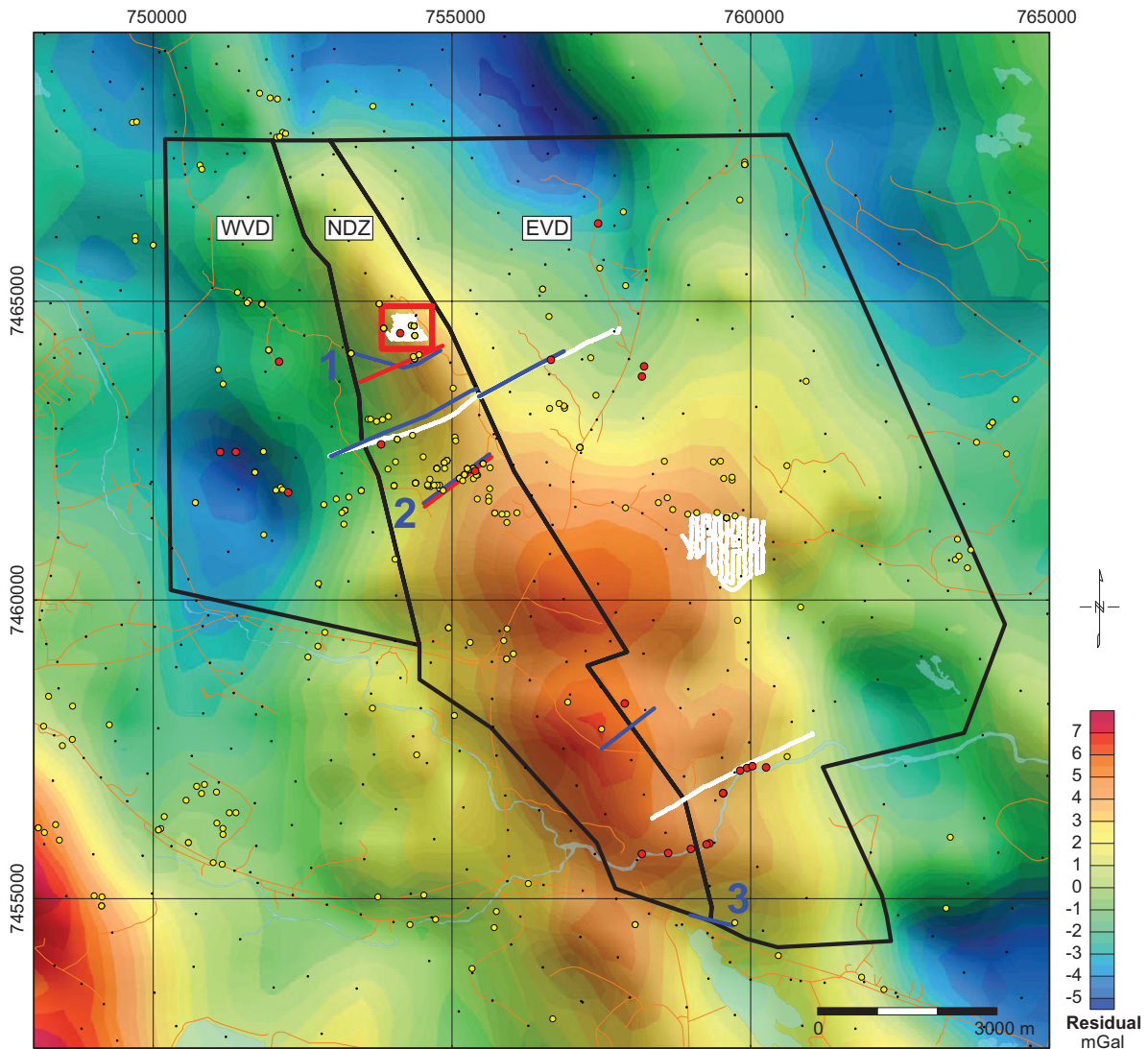


Figure 18. The residual gravity field in the Nautanen area. Black dots show the location of gravity measurements; black polygons represent study area domains. The white and blue lines represent new ground magnetic and VLF measurements, respectively (this study). The numbers "1–3" correspond to profiles discussed in the main text, and relate to Figs. 21–24. Earlier petrophysical samples are shown by yellow dots, newer samples by red dots. The red box surrounding the Nautanen deposit is presented in Figure 19; the red lines show the extent of the extracted cross-sections from 3D VOXI models shown in Figure 21 and Figure 23.

Table 4. The petrophysical properties of different rock types in the Nautanen area. The total number of petrophysical samples is 267.

Rock type	No. of samples	Density (SI) Mean	Density (SI) Std. dev.	Susceptibility $\times 10^{-5}$ (SI) min	Susceptibility $\times 10^{-5}$ (SI) max	Susceptibility $\times 10^{-5}$ (SI) median	Q-value min	Q-value max	Q-value median
Granite	13	2612	17	0	3691	1544	0.00	0.87	0.07
Metasedimentary rock	16	2836	98	18	67510	784	0.00	89.53	0.16
Gabbro-diorite	22	2903	50	27	19781	70	0.00	6.81	0.01
Sandstone	24	2768	74	12	18660	1850	0.00	8.37	0.45
Basalt-andesite	56	2847	76	44	53060	5339	0.00	16.00	0.45
Mica schist	22	2814	100	44	41430	1699	0.00	161.80	0.30
Rhyolite-dacite	18	2708	34	21	10933	1801	0.01	1.76	0.26
Amphibolite	23	2966	79	60	19031	7217	0.00	9.27	1.35
Greywacke	28	2819	92	39	14740	2157	0.00	7.18	0.65
Granodiorite	5	2714	53	21	3169	1975	0.00	1.56	0.16
Argillite	40	2754	112	234	32378	2338	0.03	79.69	0.37

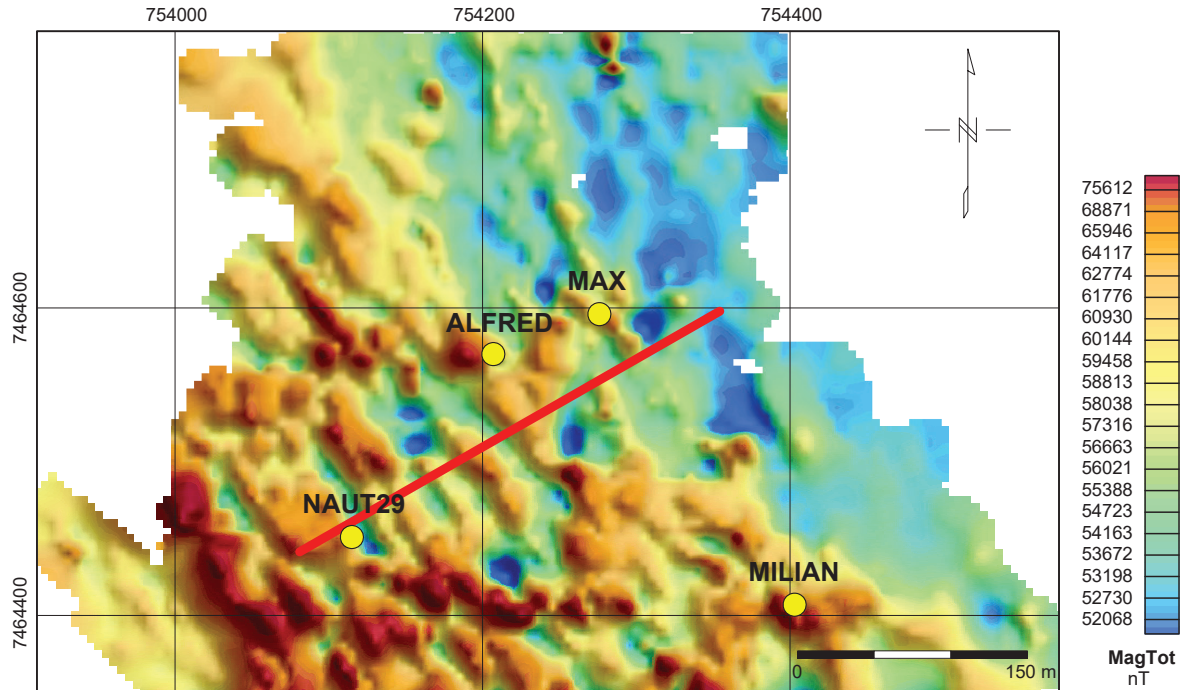


Figure 19. The total magnetic field in the area surrounding the ore deposit at Nautanen. The data is derived from ground magnetic measurements, acquired in 2014. The red profile corresponds to the cross-section from the 3D inversion shown in Figure 20.

been extracted from this 3D model, corresponding to the red profile line shown in Figure 19. The modelled cross-section shows an overturned, synformal geometry in the western part of the profile, with a southwestward-dipping axial plane, whereas the magnetic structures on the eastern side dip to the northeast (Fig. 20).

Two additional models have been made across the NDZ further south, based on ground magnetic and VLF data to visualise the geometry of the zone and interpret bedrock structures by integrating the results from both models into one comprehensive model (Figs. 21 & 22). These models correspond to the blue and red “profile 1” lines shown in Figures 17 and 18. Interpretation of resistivity cross-sections derived from VLF measurements (Figs. 22 & 24) is complicated by the fact that the measurements were made at a single frequency, and the final result is influenced by the direction of the transmitter, the signal-to-noise ratio, as well as conductors in the subsurface.

The northern part of the NDZ was the subject of ground magnetic measurements in 1977–1978. These measurements were conducted perpendicular to strike along closely spaced profiles. In general, the distance between these profiles was 80 m, but in some areas the profile spacing was reduced to 40 m. From these measurements, two 3D models have been made of shallow sub-surface conditions by inverting the gridded magnetic ground data. Results from these inversions are presented in Figure 21 and Figure 23, in which cross-sections perpendicular to the NDZ have been extracted from the 3D inversions to visualise the geometry of the magnetised sub-surface structures.

The cross-section in Figure 21 is derived from a 3D susceptibility model with an extent of 3 × 3 km. Each voxel corresponds to 25 × 25 m horizontally and 10 m vertically. 37 petrophysical samples in this area have a maximum magnetic susceptibility of 0.6 SI units. However, susceptibility is probably higher locally, so constraints on the voxels in the inversion model have been set between 0.0001 and 1 SI units.

In the cross-section shown in Figure 21 a magnetic structure in the southwest of the profile dips moderately to the southwest. A sudden break in the pattern occurs in the centre of the profile. East of this break, the highest magnetic area of the NDZ can be seen as a synformal pattern continuing towards

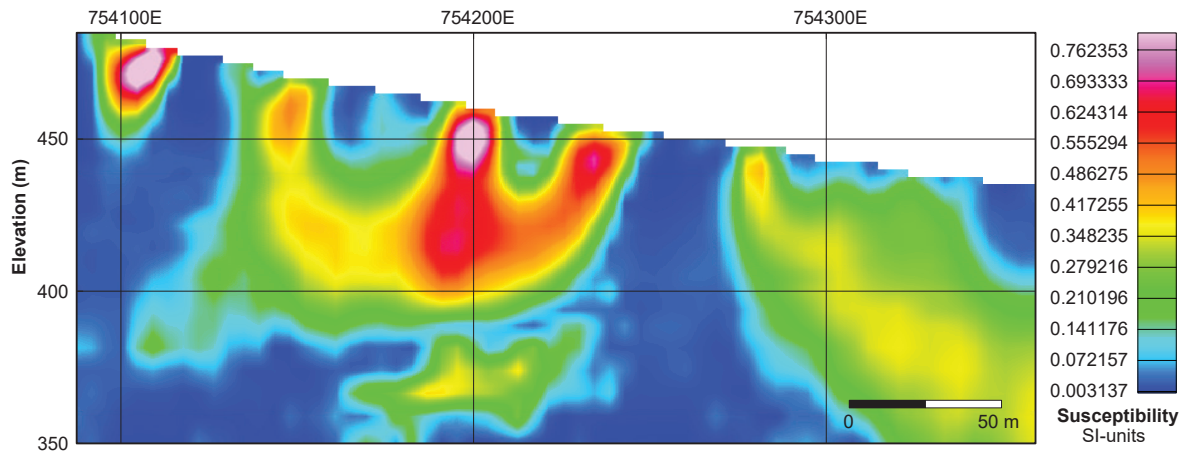


Figure 20. Susceptibility model of shallow sub-surface conditions along the cross-section shown in Figure 19. The section is derived from the 3D inversion based on ground magnetic measurements.

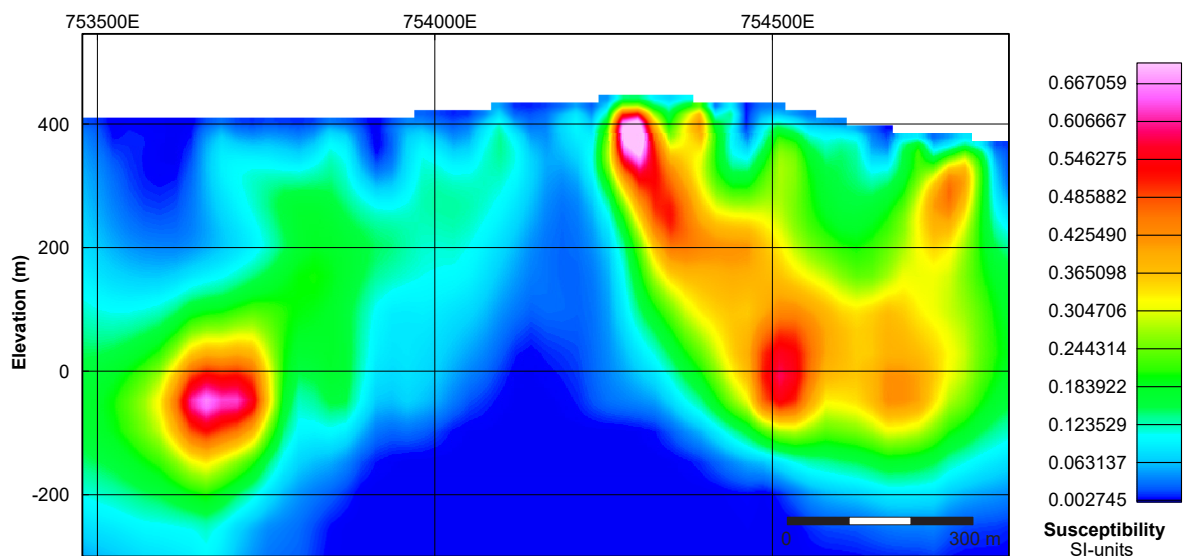


Figure 21. Cross-section from a 3D susceptibility inversion model based on gridded ground magnetic data. The lateral extent is the same as for Figure 22. Depth extent is 700 m below ground level.

the northeast. Minor magnetic structures extend up from this synformal structure towards the ground surface. These structures probably correspond to linear magnetite-rich zones.

A ground profile using a VLF instrument was carried out at roughly the same location with the aim of resolving more conductive zones in the bedrock (Fig. 22). The corresponding cross-section shows the resistivity properties of the sub-surface. Some features in the resistivity cross-section resemble those seen in the susceptibility model. For instance, more resistive west-dipping structures can be seen in the western part of the cross-section (Fig. 22). This could be a structure that has been thrust upwards from the southwest to the northeast. The structure is positioned just next to a more conductive feature, seen in the susceptibility model as a highly magnetic structure.

Another 3D susceptibility inversion model has been made of an area approximately 2 km southeast of the NDZ (Fig. 23). Its geographical extent is displayed in Figure 17 and Figure 18 as the red line marked “2”. The original model had an extent of 4×4 km; 116 petrophysical samples have been acquired from within that area. The maximum magnetic susceptibility value for these samples is 0.67 SI units.

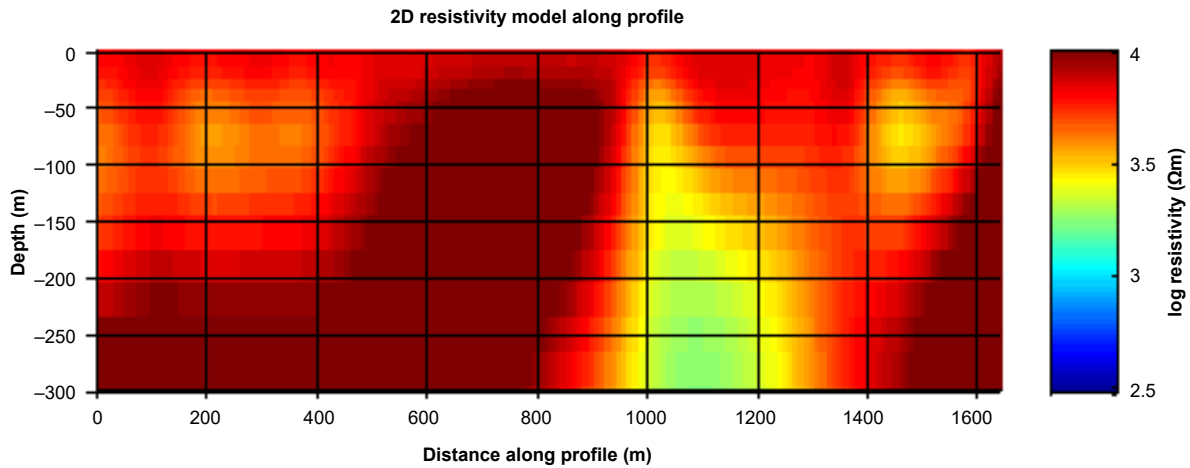


Figure 22. Inversion model based on VLF measurements along the profile labelled “1” in Figure 17 and Figure 18. It crosses the same lithological units as in Figure. 21. The model displays apparent resistivity in the ground at shallow depth.

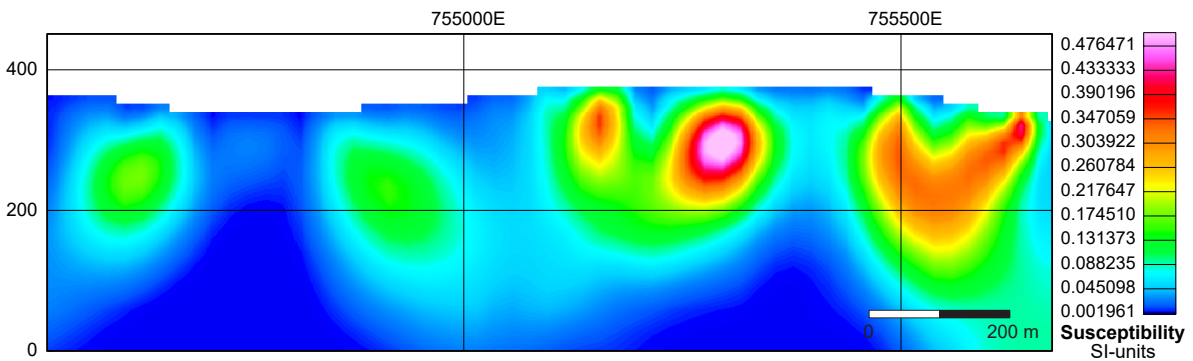


Figure 23. Cross-section derived from a 3D susceptibility inversion model based on gridded ground magnetic data. The lateral extent corresponds to profile “2” in Figure 17 and Figure 18. Depth extent is almost 400 m below ground level.

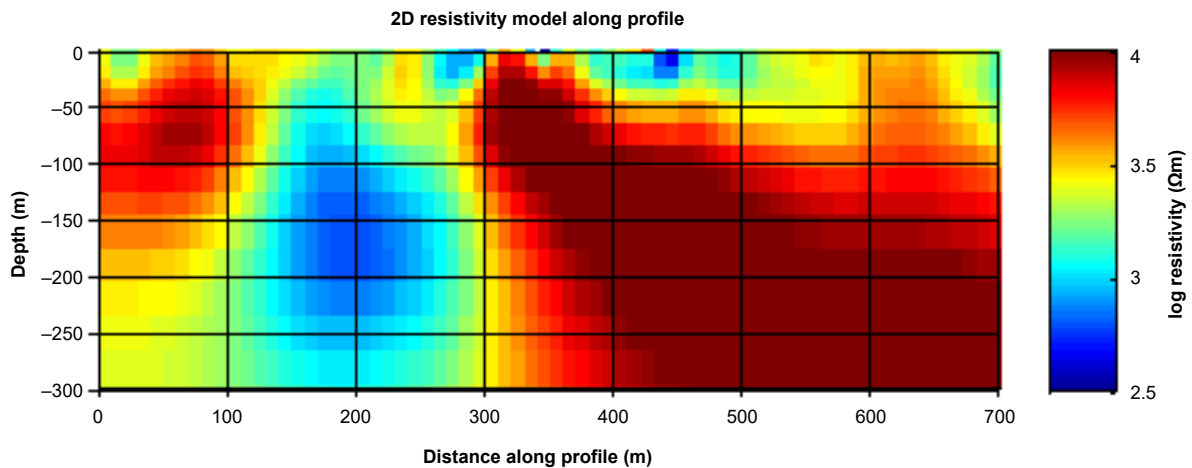


Figure 24. Resistivity cross-section derived by inverting VLF measurements along the profile labelled “3” in Figure 17 and Figure 18. The model displays apparent resistivity in the ground at shallow depth.

Thus, constraints on the voxels in the inversion model have been set between 0.0001 and 0.7 SI units. Due to the relatively small geographical extent of the model, each voxel has been given the size of 25×25 m laterally and approximately 10 m vertically at ground surface. In the eastern part of this cross-section, a magnetic anomaly with an inferred synformal shape occurs, resembling the anomaly structure seen in Figure 21.

The most southerly VLF profile was made a further 8 km to the S-SE along the NDZ (Fig. 24). The profile was made predominantly on the eastern side of the NDZ; its extent is marked with the blue profile line “3” in Figure 17 and Figure 18. A fairly broad conductive zone can be seen in the western part of this cross-section, corresponding to a low-magnetic area. In the east, a resistive feature with a relatively shallow south-eastward dip occurs (approximately 45°). This feature correlates to high-magnetic bands seen on the magnetic anomaly map (Figure. 17).

SUMMARY AND CONCLUSIONS

Bedrock and structural mapping, litho-geochemistry, U-Pb geochronology and geophysical modelling have been integrated to characterise a package of polydeformed and variably altered c. 1.88 Ga meta-volcanosedimentary rocks in the Nautanen area of northern Norrbotten. The summary and conclusions from this work are:

(1) The investigated sequence, the Muorjevaara group, consists of calc-alkaline, basaltic andesitic to mainly andesitic metavolcaniclastic and volcanogenic (epiclastic) metasedimentary rocks. Lesser intercalated and interbedded pelite, mica schist and amphibolite units occur, and gradational and layered compositional and textural variation is relatively common throughout the sequence. Locally, granitic and dioritic rocks intrude the meta-volcanosedimentary sequence. Metasomatic-hydrothermal alteration (mainly potassic-ferroan ± calcic) variably affects the meta-volcanosedimentary sequence across the study area and is most intensely developed in high-strain shear zones.

(2) U-Pb SIMS zircon dating of a meta-andesite has yielded a relatively precise U-Pb concordia age of 1878 ± 7 Ma (2σ). This date constrains the timing of syn-orogenic intermediate magmatism and provides the first absolute age for the metasupracrustal sequence hosting the Nautanen IOCG and Aitik Cu-Au-Ag deposits. The c. 1.88 Ga magmatic event coincides with regional, continental arc-related basic to intermediate magmatism occurring across northern Norrbotten. Such a setting is also supported by preliminary initial ϵ_{Nd} values ranging from -4.5 to -0.3 reported by Lynch et al. (2018a) for Nautanen-Aitik supracrustal rocks.

(3) The Nautanen area contains a variety of superimposed ductile and brittle structures formed by at least two major deformation events. The predominant structures in the area are large-amplitude folds and the composite, north-northwest-striking Nautanen deformation zone (NDZ). Locally, the NDZ transects and truncates the western limbs of the large-amplitude, moderate to tight folds consistent with a phase of late-stage shearing (cf. Luth et al. 2016).

(4) Magnetic susceptibility and VLF resistivity modelling along the Nautanen deformation zone confirm the complex nature of this composite structure. Profile 1 indicates a relatively shallow dip of the lithologies in the west of the NDZ to the southwest. In the central part of the NDZ magnetic data indicates tight folding, forming synclinal structures. These features can be seen in all cross-sections derived from the 3D models in the north of the NDZ. Further south, VLF resistivity data indicate different geometries of the resistive layers in the eastern part of the NDZ.

ACKNOWLEDGEMENTS

We thank David Drejning-Carroll (Boliden) and Dave Collar for their encouragement of this study and for interesting discussions on the geology of the Nautanen–Aitik area. Martin Whitehouse, Lev Ilyinsky and Kerstin Lindén at NordSIM (Stockholm) are gratefully acknowledged for their analytical support during SIMS analysis. Nikolaos Arvanitidis (SGU) is thanked for reviewing the manuscript.

REFERENCES

- Bark, G., Wanhainen, C. & Pålsson, B.I., 2013: Textural setting of gold and its implications on mineral processing: preliminary results from three gold deposits in northern Sweden. *Proceedings of the 12th SGA Biennial Meeting, Uppsala 1*, 302–305.
- Barton, M.D., 2014: Iron oxide (-Cu-Au-REE-P-Ag-U-Co) systems. *In: H. Holland & K. Turekian (eds.): Treatise on Geochemistry*. Elsevier, 2nd edition, volume 13, 515–541.
- Barrett, T.J. & MacLean, W.H., 1999: Volcanic sequences, lithogeochemistry, and hydrothermal alteration in some bimodal volcanic-associated massive sulfide systems. *In: C.T. Barrie & M.D. Hannington (eds.): Volcanic-associated massive sulfide deposits: processes and examples in modern and ancient environments. Reviews in Economic Geology 8*, 101–131.
- Bergman, S., Kübler, L. & Martinsson, O., 2001: Description of regional geological and geophysical maps of northern Norrbotten County. *Sveriges geologiska undersökning Ba 56*, 110 pp.
- Bergman, S., Persson P.-O. & Kübler, L., 2002: U-Pb titanite and zircon ages of the Lina granite at the type locality NW of Gällivare, northern Sweden. *Sveriges geologiska undersökning C 834*, 12–17.
- Bergman, S., Billström, K., Persson, P.-O., Skiöld, T. & Evins, P., 2006: U-Pb age evidence for repeated Palaeoproterozoic metamorphism and deformation near the Pajala shear zone in the northern Fennoscandian shield. *GFF 128*, 7–20.
- Bergman, S., Stephens, M.B., Andersson, J., Kathol, B. & Bergman, T., 2012: Sveriges berggrund. 1:1 miljon. *Sveriges geologiska undersökning K 423*.
- Carlson, C.J., 2000: Iron oxide systems and base metal mineralisation in northern Sweden. *In: T.M. Porter (ed.): Hydrothermal iron oxide copper-gold and related deposits: a global perspective*. Australian Mining Foundation, Glenside, Australia, 283–296.
- Corfu, F., Andersson, T.B. & Gasser, D., 2014: The Scandinavian Caledonides: main features, conceptual advances and critical questions. *In: F. Corfu, D. Gasser & D.M. Chew (eds.) New perspectives on the Caledonides of Scandinavia and related areas. Geological Society, London, Special Publication 390*, 9–43.
- Danielsson, S., 1985: Nautanen. Borrhälsprotokoll och analysintyg från 1985-års arbeten. *Sveriges geologiska undersökning Prap 85090*, 241 pp.
- Drejning-Carroll, D, Bauer, T., Karlsson, P., Coller, D., Nordin, R., Hitzman, M. & Allen, R., 2015: New Insight into the links between major porphyry copper, IOCG, and magnetite-apatite deposits from the Gällivare area, Northern Sweden. Society of Economic Geologists, Annual Conference 2015, Hobart, Tasmania. Program and abstracts.
- Edfelt, Å., Sandrin, A., Evins, P., Jeffries, T., Storey, C., Elming, S.A. & Martinsson, O., 2006: Stratigraphy and tectonic setting of the host rocks to the Tjärrojäkka Fe-oxide Cu-Au deposits, Kiruna area, northern Sweden. *GFF 128*, 221–232.
- Geijer, P., 1918: Nautanenområdet. En malmgeologisk undersökning. *Sveriges geologiska undersökning C 283*, 103 pp.
- Grooves, D.I., Bierlein, F.P., Meinert, L.D. & Hitzman, M.W., 2010: Iron oxide copper-gold (IOCG) deposits through Earth history: Implications for origin, lithospheric setting, and distinction from other epigenetic iron oxide deposits. *Economic Geology 105*, 641–654.
- Gustafsson, B., 1985: Fältarbeten 1984 inom delprojektområde Gällivare J Gällivare SV och SO. Slutrapport. *Sveriges geologiska undersökning Prap 85005*, 125 pp.
- Gustafsson, B., 1986: Projekt 5515 Malmberget. Prospekteringsarbeten 1985. Rekommendationer för 1986. Lägesrapport 1986-01-15. *Sveriges geologiska undersökning Prap 86004*, 220 pp.
- Gustafsson, B. & Johansson, L., 1984: Ferrum kopparfyndighet geofysik och geologi 1984. *Sveriges geologiska undersökning Prap 84158*, 18 pp.
- Hanski, E.J., 2012: Evolution of the Palaeoproterozoic (2.50–1.95) non-orogenic magmatism in the eastern part of the Fennoscandian Shield. *In: V.A. Melezhik, A.R. Prave, E.J. Hanski, A.E. Fallick, A. Lepland, L.R. Kump & H. Strauss (eds.): Reading the archive of Earth's oxygenation*, Volume 1, Springer, Berlin, 179–245.

- Hanski, E.J. & Huhma, H., 2005: Central Lapland greenstone belt. *In: R. Lehtinen, P.A. Nurmi, O.T. Rämö (eds.) Precambrian Geology of Finland – key to the evolution of the Fennoscandian Shield*. Elsevier, Amsterdam, 139–194.
- Korja, A., Lahtinen, R. & Nironen, M., 2006: The Svecofennian orogen: a collage of microcontinents and island arcs. *In: D.G. Gee & R.A. Stephenson (eds.): European lithosphere dynamics. Geological Society, London, Memoirs 32*, 561–578.
- Lahtinen, R., Korja, A. & Nironen, M., 2005: Paleoproterozoic tectonic evolution. *In: M. Lehtinen, P.A. Nurmi & O.T. Rämö (eds.): Precambrian geology of Finland – key to the evolution of the Fennoscandian Shield*. Elsevier, Amsterdam, 481–532.
- Lahtinen, R., Garde, A.A. & Melezhik, V.A., 2008: Paleoproterozoic evolution of Fennoscandia and Greenland. *Episodes 31*, 1–9.
- Lahtinen, R., Korja, A., Nironen, M. & Heikkinen, P., 2009: Paleoproterozoic accretionary processes in Fennoscandia. *Geological Society, London, Special Publications 318*, 237–259.
- Lauri, L.S., Hellström, F., Bergman, S., Huhma, H. & Lepistö, S., 2016. New insights into the geological evolution of the Archean Norrbotten province, Fennoscandian Shield. *Bulletin of the Geological Society of Finland Special Volume 1*, p. 151.
- Le Maitre, R.W., 1976: The chemical variability of some common igneous rocks. *Journal of Petrology 17*, 589–637.
- Ludwig, K.R., 2012: User's manual for Isoplot 3.75. A geochronological toolkit for Microsoft Excel. *Berkeley Geochronology Center Special Publication No. 5*, 75 pp.
- Lund, C., 2009. *Mineralogical, chemical and textural properties of the Malmberget iron deposit. A process mineralogically characterisation*. M.Sc. thesis, Luleå University of Technology, Luleå, Sweden, 98 p.
- Luth, S., Jönsson C. & Jönberger J., 2015: Integrated geological and geophysical field studies in the Livijärvi key area, Pajala region. *Sveriges geologiska undersökning report 2015:12*, 29 pp.
- Luth, S., Jönsson C., Hellström, F., Jönberger J., Djuly, T., van Assema, B. & Smoor, W., 2016: Structural and geochronological studies on the crustal-scale Pajala deformation zone, northern Sweden. *Bulletin of the Geological Society of Finland Special Volume 1*, p. 263.
- Lynch, E.P. & Jönberger, J., 2014: Summary report on available geological, geochemical and geophysical information for the Nautanen key area, Norrbotten. *Sveriges geologiska undersökning report 2014:34*, 40 pp.
- Lynch, E.P., Jönberger, J., Bauer, T.E., Sarlus, Z. & Martinsson, O., 2015: Meta-volcanosedimentary rocks in the Nautanen area, Norrbotten: Preliminary lithological and deformation characteristics. *Sveriges geologiska undersökning report 2015:30*, 51 pp.
- Lynch, E.P., Bauer, T.E., Huhma, H., Drejling-Caroll, D., 2018a: Petrogenesis of c. 1.9 Ga meta-volcanosedimentary rocks in the Nautanen-Aitik area, northern Sweden: Geological, litho-geochemical and Sm-Nd isotopic constraints. Proceedings of the 33rd Nordic Geological Winter Meeting, Copenhagen. Program and abstracts.
- Lynch, E.P., Hellström, F.A., Huhma, H., Jönberger, J., Persson, P-O. & Morris, G., 2018b: Geology, lithostratigraphy and petrogenesis of c. 2.14 Ga greenstone successions in the Nunasvaara and Masugnsbyn areas, northernmost Sweden. *In: Bergman, S. (ed): Geology of the Northern Norrbotten ore province, northern Sweden. Rapport och Meddelanden 141*, Sveriges geologiska undersökning. This volume pp 19–77.
- Martinsson, O., 1995: Greenstone and porphyry hosted ore deposits in northern Norrbotten. *PIM/NUTEK report #3*, 58 pp.
- Martinsson, O., 1997. *Tectonic Setting and Metallogeny of the Kiruna Greenstones*. Ph.D. thesis, Luleå University of Technology, Luleå, Sweden.
- Martinsson, O., 2004: Geology and metallogeny of the northern Norrbotten Fe–Cu–Au province. *In: R.L. Allen, O. Martinsson & P. Weihed (eds.): Svecofennian ore-forming environments of northern Sweden – volcanic-associated Zn–Cu–Au–Ag, intrusion-associated Cu–Au, sediment-hosted Pb–Zn, and magnetite-apatite deposits in northern Sweden. Society of Economic Geologists, guidebook series 33*, 131–148.

- Martinsson, O. & Wanhainen, C., 2004: Character of Cu-Au mineralisation and related hydrothermal alteration along the Nautanen deformation zone, Gällivare area, northern Sweden. *In*: R.L. Allen, O. Martinsson & P. Weihed (eds.): Svecofennian ore-forming environments of northern Sweden – volcanic-associated Zn-Cu-Au-Ag, intrusion-associated Cu-Au, sediment-hosted Pb-Zn, and magnetite-apatite deposits in northern Sweden. *Society of Economic Geologists, guidebook series 33*, 149–160.
- Martinsson, O. & Wanhainen, C., 2013: Fe oxide and Cu-Au deposits in the northern Norrbotten ore district. *Society of Geology Applied to Mineral Deposits (SGA) excursion guidebook SWE5*, 74 pp.
- Martinsson, O., Vaasjoki, M., Persson, P.-O., 1999: U-Pb zircon ages of Archaean to Palaeoproterozoic granitoids in the Torneträsk-Råstojaure area, northern Sweden. *Sveriges geologiska undersökning C831*, 70–90.
- Martinsson, O., Billström, K., Broman C., Weihed, P. & Wanhainen C., 2016: Metallogeny of the Northern Norrbotten ore province, northern Fennoscandian Shield with emphasis on IOCG and apatite-iron ore deposits. *Ore Geology Reviews 78*, 447–492.
- McGimpsey, I., 2010: *Petrology and lithochemisrty of the host rocks to the Nautanen Cu-Au deposit, Gällivare area, northern Sweden*. M.Sc. thesis, Lund University, Lund, Sweden, 82 pp.
- McPhie, J., Doyle, M. & Allen, R., 1993: *Volcanic textures: A guide to the interpretation of volcanic textures in volcanic rocks*. CODES Key Centre, University of Tasmania, 198 pp.
- Melezhik, V.A. & Fallick, A.E., 2010: On the Lomagundi-Jatuli carbon isotopic event: The evidence from the Kalix Greenstone Belt, Sweden. *Precambrian Research 179*, 165–190.
- Melezhik, V.A. & Hanski, E.J., 2012: The early Paleoproterozoic of Fennoscandia: Geological and tectonic settings. *In*: V.A. Melezhik, A.R. Prave, E.J. Hanski, A.E. Fallick, A. Lepland, L.R. Kump & H. Strauss (eds.): *Reading the archive of Earth's oxygenation*, Volume 1, Springer, Berlin. 33–38.
- Melezhik, V.A., Kump, L.R., Hanski, E.J., Fallick, A.E. & Prave, A.R., 2012. Tectonic evolution and major global Earth-surface palaeoenvironmental events in the Palaeoproterozoic. *In*: V.A. Melezhik, A.R. Prave, E.J. Hanski, A.E. Fallick, A. Lepland, L.R. Kump & H. Strauss (eds.): *Reading the archive of Earth's oxygenation*, Volume 1, Springer, Berlin, 3–21.
- Mellqvist, C., Öhlander, B., Skiöld, T. & Wickström, A., 1999: The Archean-Proterozoic paleoboundary in the Luleå area, northern Sweden: field and isotope geochemical evidence for a sharp terrane boundary. *Precambrian Research 96*, 225–243.
- Monro, D., 1988: *The geology and genesis of the Aitik Cu-Au deposit, arctic Sweden*. Ph.D. thesis, University College Cardiff, UK, 386 pp.
- New Boliden, 2016. *Nautanen copper-mineralization in northern Sweden*. Company press release, 05-02-2016. <www.boliden.com>
- Nironen, M., 1997: The Svecofennian orogen: a tectonic model. *Precambrian Research 86*, 21–44.
- Öhlander, B., Skiöld, T., Hamilton, P.J. & Claesson, L.-Å., 1987: The western border of the Archaean province of the Baltic Shield evidence from northern Sweden. *Contributions to Mineralogy & Petrology 95*, 437–450.
- Perdahl, J.A., 1995: *Svecofennian volcanism in northernmost Sweden*. Ph.D. thesis, Luleå University of Technology, Luleå, Sweden.
- Pitkänen, T., 1997: *Anisotropy of magnetic susceptibility of mylonites from the Kolkonjoki and Nautanen deformation zones in Norrbotten, Sweden*. M.Sc. thesis, Luleå University of Technology, Luleå, Sweden, 64 pp.
- Reddy, S.M. & Evans, D.A.D., 2009: Palaeoproterozoic supercontinents and global evolution: correlations from core to atmosphere. *In*: S.M. Reddy, R. Mazumdr, D.A.D. Evans, A.S. Collins (eds): *Paleoproterozoic supercontinents and global evolution*. Geological Society, London, *Special Publication 323*, 1–26.
- Ros, F., 1980: Nautanenområdet. Rapport över SGU:s arbeten utförda under 1966–1979. *Sveriges geologiska undersökning Brap 81530*, 33 pp.
- Sammelmin, M., 2011. *The Nature of Gold in the Aitik Cu-Au Deposit. Implications for Mineral Processing and Mine Planning*. Licentiate thesis, Luleå University of Technology, Luleå, Sweden, 67 pp.

- Sarlus, Z., 2013: *Geology of the Salmijärvi Cu-Au deposit*. M.Sc. thesis, Luleå University of Technology, Luleå, Sweden, 75 pp.
- Sarlus, Z., 2016: *Geochemical and geochronological constraints on 1.88 and 1.80 Ga magmatic events in the Gällivare area, northern Sweden*. Licentiate thesis, Luleå University of Technology, Luleå, Sweden, 106 pp.
- Sarlus, Z., Andersson, U.B., Bauer T.E., Wanhainen, C., Martinsson, O., Nordin, R., Andersson, J.B.H., 2017: Timing of plutonism in the Gällivare area: implications for Proterozoic crustal development in the northern Norrbotten ore district, Sweden. *Geological Magazine* 154, 1–26.
- Skiöld, T. & Cliff, R.A., 1984: Sm–Nd and U–Pb dating of Early Proterozoic mafic–felsic volcanism in northernmost Sweden. *Precambrian Research* 26, 1–13.
- Smith, M., Coppard J., Herrington R. & Stein H., 2007: The geology of the Rakkurijärvi Cu–(Au) prospect, Norrbotten: A new iron-oxide–copper–gold deposit in northern Sweden. *Economic Geology* 102, 393–414.
- Smith, M.P., Storey, C.D., Jefferies, T.E. & Ryan, C., 2009: In situ U–Pb and trace element analysis of accessory minerals in the Kiruna district, Norrbotten, Sweden: New constraints on the timing and origin of mineralisation. *Journal of Petrology* 50, 2063–2094.
- Smith, M.P., Gleeson S. A. & Yardley B. W. D., 2013: Hydrothermal fluid evolution and metal transport in the Kiruna District, Sweden: Contrasting metal behaviour in aqueous and aqueous–carbonic brines. *Geochimica et Cosmochimica Acta* 102, 89–112.
- Spitz, G. & Darling, R., 1978: Major and minor element lithogeochemical anomalies surrounding the Louvem copper deposit, Val d’Or, Quebec. *Canadian Journal of Earth Sciences* 15, 1161–1169.
- Stacey, J.S. & Kramers, J.D., 1975: Approximation of terrestrial lead isotope evolution by a two-stage model. *Earth and Planetary Science Letters* 26, 207–221.
- Steiger, R.H. & Jäger, E., 1977: Convention on the use of decay constants in geo- and cosmochemistry. *Earth and Planetary Science Letters* 36, 359–362.
- Storey, C.D., Smith M.P. & Jefferies T.E., 2007: In situ LA-ICP-MS U–Pb dating of metavolcanics of Norrbotten, Sweden: Records of extended geological histories in complex titanite grains. *Chemical Geology* 240, 163–181.
- Tollefsen, E., 2014: *Thermal and chemical variations in metamorphic rocks in Nautanen, Gällivare, Sweden*. M.Sc. thesis, Stockholm University, Stockholm, Sweden, 50 pp.
- Tucker, M.E., 1991: *Sedimentary petrology: An introduction to the origin of sedimentary rocks*. Blackwell Science, Oxford, 260 pp.
- Waara, S., 2016. *Garnet occurrence and its relationship to mineralization at the Nautanen deposit, northern Sweden*. M.Sc. thesis, Luleå University of Technology, Luleå, Sweden.
- Wanhainen, C., Billström, K., Stein, H., Martinsson, O. & Nordin, R., 2005. 160 Ma of magmatic/hydrothermal and metamorphic activity in the Gällivare area: Re–Os dating of molybdenite and U–Pb dating of titanite from the Aitik Cu–Au–Ag deposit, northern Sweden. *Mineralium Deposita* 40, 435–447.
- Wanhainen, C., Billström, K. & Martinsson, O., 2006. Age, petrology and geochemistry of the porphyritic Aitik intrusion, and its relation to the disseminated Aitik Cu–Au–Ag deposit, northern Sweden. *GFF* 128, 273–286.
- Wanhainen, C., Broman, C., Martinsson, O. & Magnor, B., 2012: Modification of a Palaeoproterozoic porphyry-like system: Integration of structural, geochemical, petrographic, and fluid inclusion data from the Aitik Cu–Au–Ag deposit, northern Sweden. *Ore Geology Reviews* 48, 306–331.
- Weihed, P., Arndt, N., Billström, K., Duchesne, J.-C., Eilu, P., Martinsson, O., Papunen, H. & Lahtinen, R., 2005: Precambrian geodynamics and ore formation: The Fennoscandian Shield. *Ore Geology Reviews* 27, 273.
- White, J.D.L. & Houghton, B.F., 2006: Primary volcanoclastic rocks. *Geology* 34, 677–680.
- Whitehouse, M.J. & Kamber, B.S., 2005: Assigning dates to thin gneissic veins in high-grade metamorphic terranes: a cautionary tale from Akilia, southwest Greenland. *Journal of Petrology* 46, 291–318.

- Whitehouse, M.J., Claesson, S., Sunde, T. & Vestin, J., 1997: Ion-microprobe U–Pb zircon geochronology and correlation of Archaean gneisses from the Lewisian Complex of Gruinard Bay, north-west Scotland. *Geochimica et Cosmochimica Acta* 61, 4429–4438.
- Whitehouse, M.J., Kamber, B.S. & Moorbath, S., 1999: Age significance of U–Th–Pb zircon data from Early Archaean rocks of west Greenland: a reassessment based on combined ion-microprobe and imaging studies. *Chemical Geology* 160, 201–224.
- Wiedenbeck, M., Alle, P., Corfu, F., Griffin, W.L., Meier, M., Oberli, F., Quadt, A.V., Roddick, J.C. & Spiegel, W., 1995: Three natural zircon standards for U–Th–Pb, Lu–Hf, trace element and REE analysis. *Geostandards Newsletter* 19, 1–23.
- Wiedenbeck, M., Hanchar, J.M., Peck, W.H., Sylvester, P., Valley, J., Whitehouse, M., Kronz, A., Morishita, Y., Nasdala, L., Fiebig, J., Franchi, I., Girard, J.P., Greenwood, R.C., Hinton, R., Kita, N., Mason, P.R.D., Norman, M., Ogasawara, M., Piccoli, P.M., Rhede, D., Satoh, H., Schulz-Dobrick, B., Skår, O., Spicuzza, M.J., Terada, K., Tindle, A., Togashi, S., Vennemann, T., Xie, Q. & Zheng, Y.F., 2004: Further characterisation of the 91500 zircon crystal. *Geostandards and Geoanalytical Research* 28, 9–39.
- Williams, P.J., 2010: "Magnetite-group" IOCGs with special reference to Cloncurry (NW Queensland) and northern Sweden: settings, alteration, deposit characteristics, fluid sources, and their relationship to apatite-rich iron ores. In: L. Corriveau & H. Mumin (eds.): *Exploring for iron oxide copper-gold deposits: Canada and global analogues*. Geological Association of Canada Short Course 20, 23–38.
- Winchester, J.A. & Floyd, P.A., 1977: Geochemical discrimination of different magma series and their differentiation products using immobile elements. *Chemical Geology* 20, 325–343.
- Witschard, F., 1970: Description of the geological maps Lainio NV, NO, SV, SO with an appendix by P. Niskanen the aeromagnetic maps Lainio NV, NO, SV, SO. *Sveriges geologiska undersökning Af* 9–12, 116 p.
- Witschard, F., 1996: Berggrundskartan 28K Gällivare NO, NV, SO, SV. 1:50 000-scale maps. *Sveriges geologiska undersökning Ai* 98–101. (With a description in English).
- Zweifel, H., 1976: Aitik. Geological documentation of a disseminated copper deposit. *Sveriges geologiska undersökning C* 720, 80 pp.



Geological Survey of Sweden
Box 670
SE-751 28 Uppsala
Phone: +46 18 17 90 00
Fax: +46 18 17 92 10
www.sgu.se

Uppsala 2018
ISSN 0349-2176
ISBN 978-91-7403-393-9
Tryck: Elanders Sverige AB